Inorganic Chemistry

pubs.acs.org/IC Article

(1,2-Azole)bis(bipyridyl)ruthenium(II) Complexes: Electrochemistry, Luminescent Properties, And Electro- And Photocatalysts for CO₂ Reduction

Elena Cuéllar, Laura Pastor, Gabriel García-Herbosa, John Nganga, Alfredo M. Angeles-Boza, Alberto Diez-Varga, Tomás Torroba, Jose M. Martín-Alvarez, Daniel Miguel, and Fernando Villafañe*



Cite This: Inorg. Chem. 2021, 60, 692-704



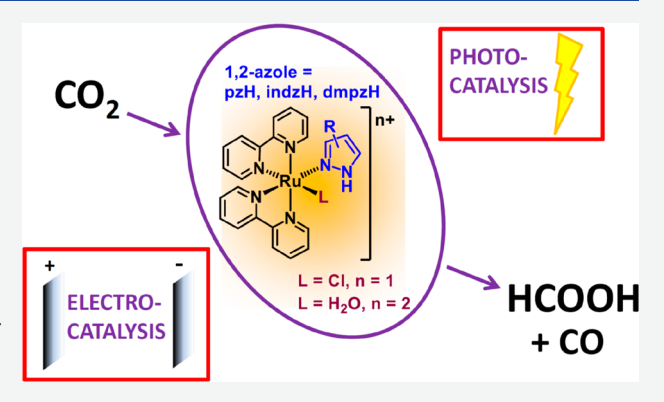
ACCESS

III Metrics & More

Article Recommendations

Supporting Information

ABSTRACT: New *cis-*(1,2-azole)-aquo bis(2,2'-bipyridyl)-ruthenium(II) (1,2-azole (az*H) = pzH (pyrazole), dmpzH (3,5-dimethylpyrazole), and indzH (indazole)) complexes are synthesized via chlorido abstraction from *cis-*[Ru(bipy)₂Cl(az*H)]OTf. The latter are obtained from *cis-*[Ru(bipy)₂Cl₂] after the subsequent coordination of the 1,2-azole. All the compounds are characterized by ¹H, ¹³C, ¹⁵N NMR spectroscopy as well as IR spectroscopy. Two chlorido complexes (pzH and indzH) and two aquo complexes (indzH and dmpzH) are also characterized by X-ray diffraction. Photophysical and electrochemical studies were carried out on all the complexes. The photophysical data support the phosphorescence of the complexes. The electrochemical behavior of all the complexes in an Ar atmosphere indicate that the oxidation processes assigned to



 $Ru(II) \rightarrow Ru(III)$ occurs at higher potentials in the aquo complexes. The reduction processes under Ar lead to several waves, indicating that the complexes undergo successive electron-transfer reductions that are centered in the bipy ligands. The first electron reduction is reversible. The electrochemical behavior in CO_2 media is consistent with CO_2 electrocatalyzed reduction, where the values of the catalytic activity $[i_{cat}(CO_2)/i_p(Ar)]$ ranged from 2.9 to 10.8. Controlled potential electrolysis of the chlorido and aquo complexes affords CO and formic acid, with the latter as the major product after 2 h. Photocatalytic experiments in MeCN with $[Ru(bipy)_3]Cl_2$ as the photosensitizer and TEOA as the electron donor, which were irradiated with >300 nm light for 24 h, led to CO and HCOOH as the main reduction products, achieving a combined turnover number $(TON_{CO+HCOO}^-)$ as high as 107 for 2c after 24 h of irradiation.

■ INTRODUCTION

Two of the most important global problems, i.e., the need for renewable energy sources and the rising levels of atmospheric CO_2 , might be solved by accessing the efficient and selective catalytic reduction of CO_2 . Different molecular catalysts have been investigated over past years, generating an extensive catalog of metal complexes with electrochemical or photochemical activity for CO_2 reduction. The electrochemical CO_2 reduction catalyzed by cis-[Ru(bipy) $_2(CO)_2$] $^{2+}$ and cis-[Ru(bipy) $_2(CO)CI$] $^+$ (bipy = 2,2'-bipyridine) was one of the first systems reported back in 1987. Since then, a plethora of Ru(II) catalysts have been described in the context of CO_2 catalytic reduction.

The most extensively used system in this field is *cis*[Ru(bipy)₂(CO)L]ⁿ⁺ (L = H, CO₂, C(O)OH, or CO and n = 1 or 2)¹⁰ (A in Chart 1). These catalysts were first introduced by Tanaka et al. $^{9,11-13}$ and were then also developed by other research groups, such as those of Meyer, $^{14-16}$ Lehn, 17,18 Fujita, 19 and Ishida. 20 These complexes are electrochemically

active and readily react with carbon dioxide to form formic acid and carbon monoxide.

Tanaka's group²¹ recently broadened the variety of compounds to those of the type $[Ru(tpy^*)(bipy^*)L]^{n+}$ (tpy* = 2,2':6',2"-terpyridine or substituted derivatives; bipy* = bipy or substituted derivatives; L = CO, MeCN, or Cl; and n = 1 or 2) (C in Chart 1). These catalysts were further investigated by Meyer,^{22,23} Fujita,²⁴ Ott,^{25–27} and Angeles-Boza.²⁸ Related complexes where one of the coordinating atoms in the bidentate ligand is not a nitrogen atom have been developed by Masaoka^{29,30} and Miller³¹ (D in Chart 1, where L = carbene or phosphine).

Received: September 12, 2020 Published: December 24, 2020





Chart 1. Ru(II) Complexes Studied As Catalysts for CO₂ Reduction Based On "cis-Ru^{II}(bipy)₂" Fragments (A and B) and Ru^{II}(tpy)(bipy) (C and D)^a

^aL = ligand, S = solvent or labile ligand.

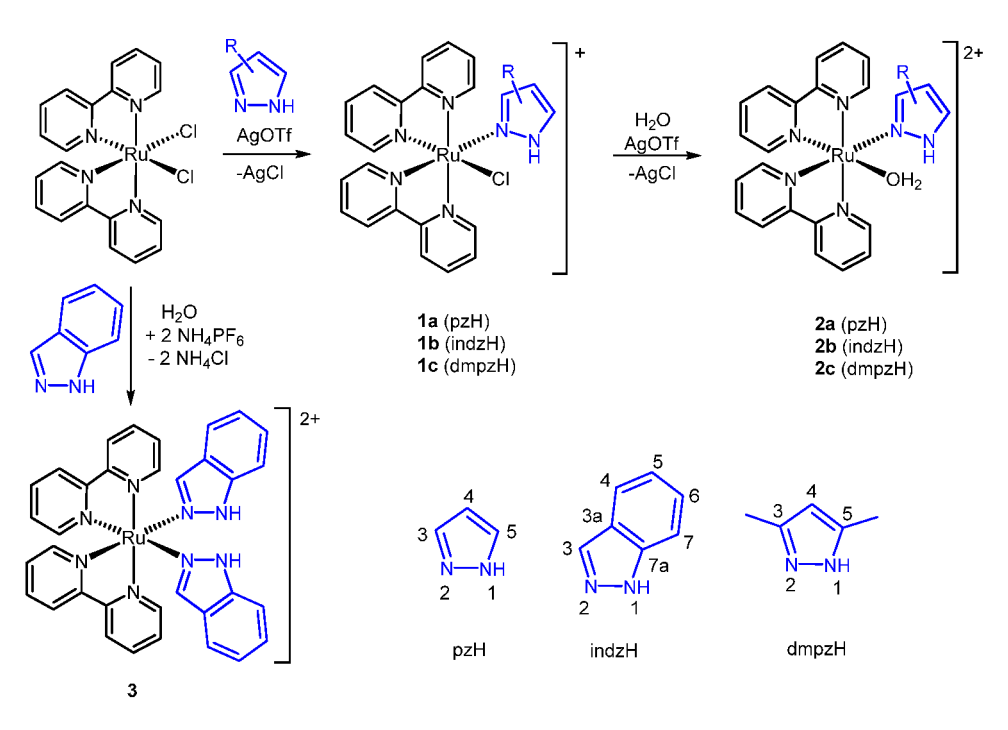
The system by far less explored results from the coordination of a N-donor monodentate ligand to the "cis-Ru(bipy)₂" fragment to give complexes of the type cis-

D

[Ru(bipy)₂LS]ⁿ⁺, (**B** in Chart 1; L = N-donor monodentate ligand, S = solvent or labile ligand, and n = 1 or 2). This strategy could generate complexes such as those containing the "Ru^{II}(bipy)(tpy)" moiety but by easier and more straightforward synthetic procedures. Surprisingly, we have been able to find only one precedent in the literature for complexes **B** in Chart 1 by J. Chen, who described complexes of the type *cis*[Ru(bipy)₂LX]⁺ (X = H, formate, or dithioformate) and *cis*[Ru(bipy)₂L(NCMe)]²⁺ where L is a monodentate phosphine.³²

This work reports a further contribution to this scarcely explored option where the chosen ligand L in B is a 1,2-azole ligand. One of the main aspects of interest in regard to these ligands is the presence of an acidic N-bound hydrogen. The role of acidic hydrogens in the "cis-Ru^{II}(bipy)₂" moiety has been widely explored, ^{33,34} and some recent studies describe the role of pH sensitive ligands, ^{35–38} the complexes' behavior in anion recognition, ^{39–43} or their DNA binding properties, ^{44,45} to name but a few. However, there are very scarce reports of complexes containing the bis(bipyridyl)ruthenium(II) fragment with 1,2-azole ligands. The landmark report of T. J. Meyer's group in 1979 on cis[Ru(bipy)₂(pzH)₂]²⁺ complexes and their deprotonated derivatives was recently revisited by Hirahara et al, who reported the role of intramolecular hydrogen bonding in the monocationic deprotonated complex on the photosubstitution reactions. ⁴⁷ The acid—base properties of [Ru(bipy)₂Cl(pzH)]⁺ and the photoreactivity and

Scheme 1. Synthesis of the Complexes Herein Described and 1,2-Azole Derivatives Used Including the Numbering for NMR Assignment



	pzH	indzH	dmpzH
cis-[Ru(bipy) ₂ Cl(az*H)]OTf	1a ⁴⁸	1b ⁴⁹	1c ⁴⁸
$\textit{cis}\text{-}[Ru(bipy)_2(H_2O)(az^*H)](OTf)_2$	2 a	2 b	2 c
cis-[Ru(bipy) ₂ (indzH) ₂](PF ₆) ₂		3	

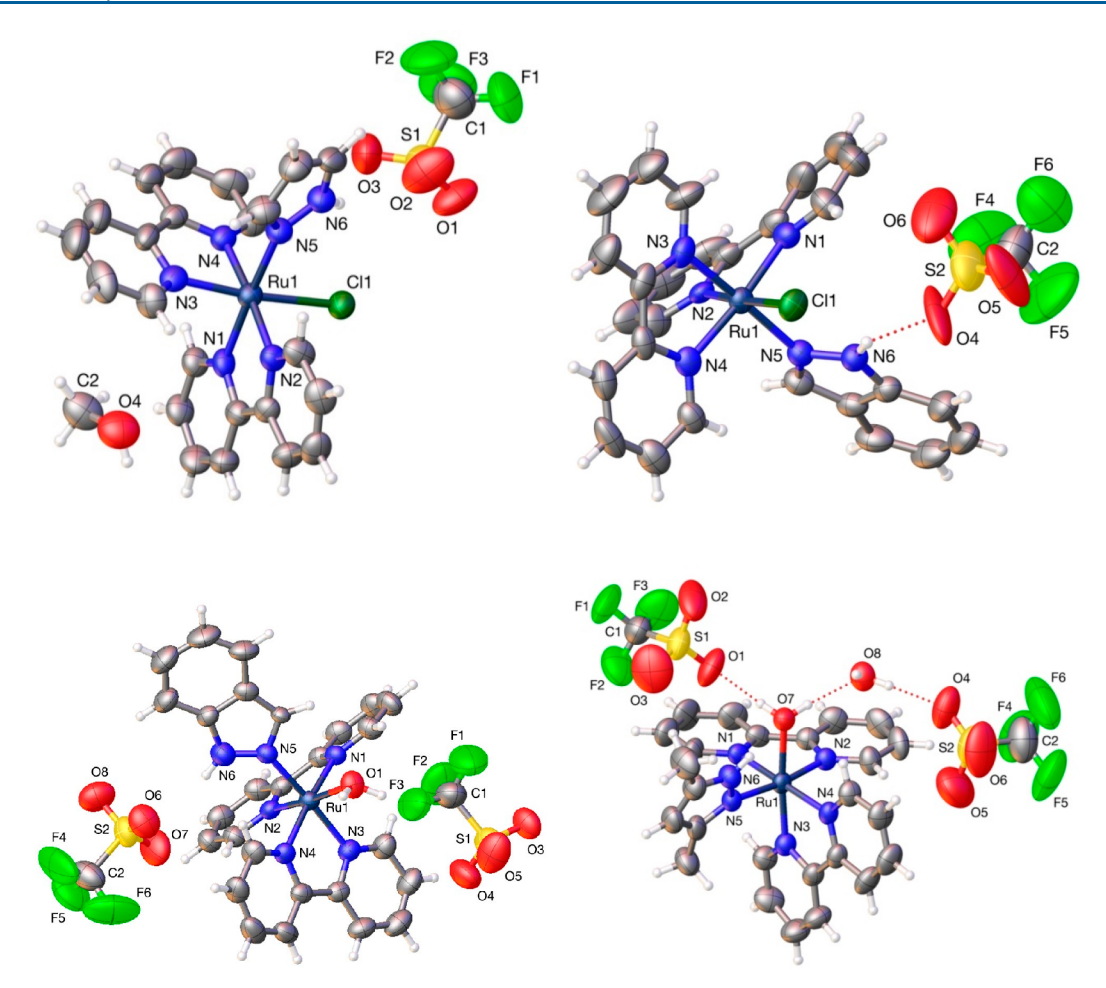


Figure 1. Perspective views with atom numbering of cis-[Ru(bipy)₂Cl(pzH)]OTf, 1a; cis-[Ru(bipy)₂Cl(indzH)]OTf, 1b; cis-[Ru(bipy)₂(H₂O)-(indzH)](OTf)₂, 2b (one of the molecules in the crystal); and cis-[Ru(bipy)₂(H₂O)(dmpzH)](OTf)₂, 2c. Thermal ellipsoids are drawn at 50% probability. Hydrogen bonds only shown for 1a and 2c for clarity.

biological studies of $[Ru(bipy)_2Cl(pzH)]^+$ have been also described. As,49 Therefore, we focused our interest on complexes of the type B in Chart 1 where L is a 1,2-azole ligand and studied their physical and chemical properties. We hypothesize that the presence of the 1,2-azole ligand will favor CO_2 activation given the ability of these ligands to hydrogen bond. In addition, the use of 1,2-azole ligands will favor the future tunability of the complexes in both ground and excited states. We have shown how a systematic control of the electronic and steric properties of other metal transition complexes containing 1,2-azoles and their derivatives that allows to tune properties of interest, such as their selectivity toward anions, their luminescent properties, 51,52 or their activity as electrocatalysts in CO_2 reduction.

Herein we report the synthesis and a thorough characterization of new (1,2-azole)-aquo bis(bipyridyl)ruthenium(II) complexes. The complete characterization of the (1,2-azole)-chlorido precursors is also described. The 1,2-azole derivatives used in this work are pyrazole (pzH), indazole (indzH), and 3,5-dimethylpyrazole (dmpzH). The electrochemical behavior of the complexes were studied, including the behavior of the complexes synthesized as electrocatalysts for the reduction of ${\rm CO}_2$. This study also includes the characterization and quantification of the products formed in the reduction of ${\rm CO}_2$ catalyzed by these complexes (CO vs formic acid). We also studied the photophysical behavior of all the complexes

obtained and their use as photocatalysts for the reduction of CO_2 .

■ RESULTS AND DISCUSSION

Synthesis and Characterization of the Complexes, All the complexes investigated in this work and their syntheses are collected in Scheme 1. A panel of complexes with different substituents was synthesized to confirm the synthetic method and also to study the influence of the substituents on the electrocatalytic reduction of CO₂. The mixed (1,2-azole)chlorido complexes cis-[Ru(bipy)₂Cl(az*H)]OTf (1) (az* = pz, dmpz, or indz; Scheme 1) and the (1,2-azole)-aquo complexes cis-[Ru(bipy)₂(H₂O)(az*H)](OTf)₂ (2) are included in Scheme 1. The pzH (1a) and dmpzH (1c) chlorido complexes were previously reported by Jude et al.,48 and the indzH (1b) complex was previously reported by Fonteles et al.; 49 however, we herein describe a new synthetic procedure and report a thorough characterization. The complex cis- $[Ru(bipy)_2(indzH)_2](PF_6)_2$ (3) is included here for comparative purposes and was synthesized by the method described by Sullivan et al. for the similar bis(pyrazole) complex.46

Chlorido complexes 1 were obtained from cis- $[RuCl_2(bipy)_2]$ by abstracting one of the chlorido ligands with the stoichiometric amount of AgOTf and the subsequent addition of the 1,2-azole. The abstraction of the second

chlorido ligand in the presence of H_2O leads to the aquo complexes 2a, 2b, and 2c.

The spectroscopic (¹H, ¹³C, and ¹⁵N NMR as well as FTIR) and analytical data support the proposed geometries and are included in the Experimental Section. Furthermore, complexes 1a, 1b, 2b, and 2c were characterized by single-crystal X-ray diffraction studies (Figure 1). The distances and angles (CCDC 2031192-2031195) are similar to those found in other 1,2-azole ruthenium(II) complexes. 54,55 In complexes 1a and 1b, the N-bound hydrogens of the pzH or indzH ligands are involved in hydrogen bonding with the oxygen atom of an OTf anion. The distances and angles determined for 1a (H(6)···O(2) 2.269(9) Å, N(6)···O(2) 2.961(10) Å, and $N(6)-H(6)\cdots O(2)$ 123.2(4)°) and 1b $(H(6)\cdots O(4)$ 1.961(16) Å, N(6)···O(4) 2.852(17) Å, and N(6)-H(6)··· O(4) 143.1(5)°) may be considered "moderate" hydrogen bonds. Moreover, in complexes 2b and 2c both hydrogens of the aquo ligands are involved in hydrogen bonding with the oxygen atom of an OTf anion and the oxygen atom of a solvent molecule (acetone in one cationic Ru complex in 2b, a molecule of water in the cases of the other Ru complex in 2b and 2c). The distances and angles detected for 2b (H(1A)... O(16) 1.734(9) Å, $O(1) \cdots O(16)$ 2.657(8) Å, and O(1)H(1A)···O(16) 167.4(4)°; H(1B)···O(13) 1.828(5) Å, O(1)··· O(13) 2.736(4) Å, and $O(1)-H(1B)\cdots O(13)$ 161.8(2)°; H(2A)···O(15) 1.739(9) Å, O(2)···O(15) 2.676(8) Å, and $O(2)-H(2A)\cdots O(15)$ 176.8(5)°; and $H(2B)\cdots O(3)$ 1.777(7) Å, $O(2)\cdots O(3)$ 2.711(6) Å, and $O(2)-H(2B)\cdots O(3)$ 173.0(3)°; O(3) and O(13) are triflate oxygens, O(15) belongs to a water molecule, and O(16) belongs to acetone) and for 2c (H(7)··O(1) 1.757(7) Å, O(7)···O(1) 2.674(9) Å, and O(7)-H(7)···O(1) 164.7(4)° and H(7)··O(8) 1.884(5) Å, $O(7)\cdots O(8)$ 2.693(6) Å, and $O(7)-H(7)\cdots O(8)$ 142.9(4)°) may also be considered "moderate" hydrogen

Electrochemical Studies. The (1,2-azole)-chlorido complexes **1a**, **1b**, and **1c** as well as the (1,2-azole)-aquo complexes **2a**, **2b**, and **2c**, showed, by cyclic voltammetry, an electrochemical behavior consistent with CO_2 activation, i.e., electrocatalyzed reduction (see the Supporting Information). As a representative example, the results registered for the complex cis-[Ru(bipy)₂(H₂O)(IndzH)](OTf)₂ **2b** are shown in Figure 2. Black (Ar) and red (CO_2) traces overlap completely in the range from -2.2 V to 0.0 V. Changing the atmosphere from Ar to CO_2 leads to a large enhancement of the current at potentials below -2.2 V.

The cyclic voltammetry data for the chlorido complexes were previously reported, although the pyrazole and dimethylpyrazole complexes were referenced to SCE^{48} whereas the indazole complex was referenced to the AgCl/Ag electrode.⁴⁹ For this reason we again studied the electrochemistry of all the complexes to reference them to the redox pair ferrocenium/ferrocene, following the IUPAC recommendations (Table 1).⁵⁶ To understand the exact role of the 1,2-azole ligands in the electrocatalyzed reduction process, the electrochemistry of complexes containing two 1,2-azoles, that is, cis-[Ru(bipy)₂(indzH)₂](PF₆)₂ (3), and no 1,2-azoles, that is, cis-[Ru(bipy)₂(NCMe)₂](PF₆)₂ (4) was also studied. The synthesis and electrochemistry under N₂ of the latter has already been described.⁵⁷

None of these previous electrochemical studies carried out on the (1,2-azole)-chlorido complexes 1 or on the bis-(acetonitrile) complex 4 described their behavior in a CO_2

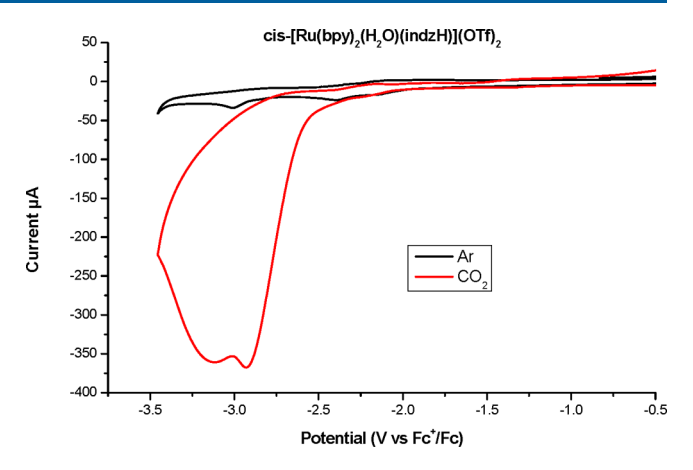


Figure 2. Cyclic voltammograms of 0.5 mM cis-[Ru(bipy)₂(H₂O)-(indzH)](OTf)₂ (2b) (3.0 mm diameter glassy carbon working electrode dish, dry MeCN, and 0.1 M Bu₄NPF₆) under Ar (black) and after bubbling CO₂ (red).

atmosphere. The ratio $\frac{i_{\rm cat}({\rm CO_2})}{i_{\rm p}({\rm Ar})}$ (Table 1) allows us to compare

the catalytic activity of the complexes, and the values obtained for the 1,2-azole complexes range from 2.9 to 10.8 (2.1 for the bis(acetonitrile) complex 4). A silver wire was used in the first scan as a pseudoreference electrode, and in the following scans the AgCl/Ag (3 M NaCl) reference electrode was used. Ferrocene was always added as internal calibrant in the last experimental measurement.

For comparative and organizational purposes, in this section we discuss first the electrochemical behavior of the (1,2-azole)-chlorido complexes 1, followed by the discussion of the (1,2-azole)-aquo complexes 2, and finally a discussion of of *cis*[Ru(bipy) $_2$ L $_2$] $^{2+}$ [L = indzH (3) or NCMe (4)]. For each complex, the electrochemistry under an Ar atmosphere is discussed prior to the behavior under a CO_2 atmosphere.

Electrochemical Behavior of Complexes 1. One reversible wave at 0.62 V was detected for 1a under GC/acetonitrile (Figure S1) whereas 1b and 1c display reversible waves at 0.33 V (Figure S3 and S7) (Table 1). These reversible oxidations are assigned to the Ru(II)/Ru(III) oxidation and occur at higher potentials than the Ru(II)/Ru(III) oxidation of cis- $[\tilde{Ru}(bipy)_2Cl_2]$ (-0.06 vs Fc⁺/Fc). This is to be expected after the substitution of the anionic electron-donating chlorido ligand by the neutral π -accepting 1,2-azole ligand and the subsequent electrostatic effect of changing from neutral to cationic complexes. However, explaining the difference in the potential (ca. 0.3 V) between the pzH complex 1a vs that of the indzH and dmpzH complexes 1b and 1c might be related to the fact that 1,2-azoles are deprotonable ligands. In this case, the oxidation of Ru(II) might involve PCET (proton-coupled electron transfer) processes with concomitant potential shifts depending on the coordinated ligand. 60,61

Scanning the chlorido complexes 1 to negative potentials under Ar (Table 1, Figures S2, S4, S6, and S8) leads to several waves, indicating that the complexes undergo successive electron-transfer reductions. This electrochemical behavior is similar to that shown by other bis(bipyridine)ruthenium(II) complexes and has been previously attributed to reduction processes centered at the bipyridine ligands. 49,59,62–64 However, all the complexes herein reported show a slight decrease (ca. 0.2–0.3 V) with respect to the reduction potentials of previously reported Ru(II) complexes able to

Table 1. Electrochemical Data Obtained by Cyclic Voltammetry in This Study and Referenced to the Redox System Ferrocenium/Ferrocene^a

	Observed $E_{ m pk}^{ m ox}$ and $E_{ m pk}^{ m red}$ values b							
Complex	Anodic scan	Cathodic scan				$i_p(Ar)^c$	$i_{cat}(CO_2)^c$	ratio $i_{cat}(CO_2)/i_p(Ar)^d$
1a	0.62 ^e	-2.05 ^e	-2.29^{e}	-2.90 ^e		-48	-223	4.6
1b	0.33 ^e	-2.00^{e}	-2.23^{e}	-2.87 ^e		-47	-138	2.9
1c	0.33 ^e	-1.97^{e}	-2.19^{e}	-2.89^{e}		-42	-132	2.9
2a	0.52 ^e	-2.04^{e}	-2.37^{e}	-2.99^{e}		-37	-297	8.0
2b	0.54 ^e	-2.04^{e}	-2.30^{e}	-2.93^{e}		-34	-368	10.8
2c	0.58 ^e	-2.18^{e}	-2.38^{e}	-3.02^{e}		-29	-188	6.5
3	0.73 ^e	-2.08^{e}	-2.32^{e}	-2.92	-3.00	-36	-179	5.0
4	1.06 ^e	-1.76^{e}	-1.95 ^e	-2.60		-62	-130	2.1

^aThe reduction potential mean value observed for ferrocenium/ferrocene (Fc⁺/Fc) used as an internal calibrant under the employed experimental conditions was $E^{\circ} = 0.443 \pm 0.005$ V vs the AgCl/Ag (3 M NaCl) electrode. ^bAnodic or cathodic scan peaks were observed under Ar unless stated otherwise. ^cMaximum registered cathodic current (μA) under Ar ($i_p(Ar)$) or CO₂ ($i_{cat}(CO_2)$). ^dRatio between the Faradaic currents observed under Ar ($i_p(Ar)$) and CO₂ ($i_{cat}(CO_2)$). ^eWaves where both peaks i_{ox} and i_{red} were observed. The value of $E_{1/2}$ is given in those cases.

electrocatalyze CO_2 reduction. $^{9,10,19-28,11,29-31,12-18}$ This slight decrease is to be expected considering the fact that most of the previously reported electrocatalysts are Ru(II) complexes that contain a CO ligand(s), which is more π -accepting and facilitates reduction. To check the reversibility of these reductions, cyclic voltammograms at different rates were recorded for 1b (Figure SS). The experiment clearly indicates that the first reduction is reversible (the second and third reductions in 1b seem to overlap; compare Figures S4 and SS).

An intense enhancement of the cathodic current is observed when the same scan is repeated under a CO_2 atmosphere. For $\mathbf{1a}$ (Figure S2), the maximum cathodic current under CO_2 is found at -3.00 V (vs Fc^+/Fc). At this potential, the ratio of the cathodic currents is $\frac{i_{\text{cat}}(CO_2)}{i_p(Ar)} = 4.6$. For $\mathbf{1b}$ and $\mathbf{1c}$ (Figures S6 and S8, respectively), the maximum cathodic currents under CO_2 were found at -2.73 and -2.94 V (vs Fc^+/Fc),

currents is $\frac{i_{\rm cat}({\rm CO}_2)}{i_p({\rm Ar})}=2.9$ in both cases. The different shapes of the waves associated with the electrocatalytic reduction of ${\rm CO}_2$ come from the competition at the electrode surface between ${\rm CO}_2$ consumption (related to the rate-determing step of the catalytic cycle) and the arrival of a new substrate by diffusion.⁴

respectively. At these potentials, the ratio of the cathodic

Electrochemical Behavior of Complexes 2. At positive potentials, the cyclic voltammograms of 2a (Figure S9), 2b (Figure S11), and 2c (Figure S16) show reversible waves at 0.52, 0.54, and 0.58 V (vs Fc⁺/Fc) respectively, that are assigned to the Ru(II)/Ru(III) oxidation. These oxidation potentials are higher than those of the respective chlorido complexes, as expected after the substitution of the anionic electron-donating chlorido ligand by the neutral σ -donating aquo ligand. Weak irreversible oxidations at slightly higher potentials were detected for some of these complexes (more clearly for 2c, see Figure S16). The presence of an aquo ligand and the high charge of the complexes after the Ru(II)/Ru(III) oxidation might facilitate the deprotonation of the aquo ligand. However, no further experiments were done to identify the species responsible for these weak waves since these processes occur during oxidation and their catalytic activity is related to the reduction processes. Complexes 1, 2, and 3 are stable in

MeCN solutions when no potential is applied, as confirmed by ¹H NMR spectra in CD₃CN even after 24 h at rt.

Scanning to negative potentials under Ar (Figures S10, S12, S15, and S17) allows us to observe several waves as the result of successive electron-transfer reductions. Cyclic voltammograms at different rates were recorded for **2b** (Figure S13 and S14) to check the reversibility of these reductions. As for **1b**, the results indicate again that the first reduction is reversible. Again, intense enhancements of the cathodic currents were detected when the same scan was carried out under a CO_2 atmosphere. The maximum cathodic current under CO_2 was found at -3.20, -2.92, and -3.13 V (vs Fc⁺/Fc) for **2a**, **2b**, and **2c**, respectively. At this potential, the ratio of the cathodic currents $\frac{i_{cat}(CO_2)}{i_p(Ar)}$ is 8.0 for **2a**, 10.8 for **2b**, and 6.5 for **2c**.

Electrochemical Behavior of Complexes 3 and 4. As indicated above, the dicationic complex cis-[Ru-(bipy)₂(indzH)₂](PF₆)₂ (3) was synthesized and studied to determine the exact role of the 1,2-azole ligands in this electrocatalyzed reduction process. The synthesis and electrochemistry of the similar bis(pyrazole) complex has been already described. 46 Compound 3 shows a reversible wave at 0.73 V (vs Fc^+/Fc) corresponding with the Ru(II)/Ru(III)oxidation (Table 1, Figure S18). As reported for the similar bis(pyrazole) complex, 46 a less intensive wave at 0.38 V (vs Fc⁺/Fc) is also visible, which is assigned to the oxidation of the deprotonated monocationic cis-[Ru(bipy)2(indz)(indzH)]PF6 complex formed in situ.⁶⁵ As for complexes 1 and 2, scanning to negative potentials under Ar (Table 1, Figures S19, and S20) leads to several waves, indicating that 3 undergoes successive electron transfer reductions attributed to reduction processes centered at the bipyridine ligands as indicated above. Again, the cyclic voltammograms recorded at different rates for 3 (Figure S20) support that the first reduction is reversible. Finally, the electrochemical behavior in CO₂ media (Table 1, Figure S21) is also consistent with a CO₂ electrocatalyzed reduction, where the value of the catalytic activity $\frac{i_{cat}(CO_2)}{i_n(Ar)}$ is 5,

a similar value to those obtained for the complexes 1 and 2, which contain only one 1,2-azole ligand each.

The electrochemical behavior in CO_2 of the bis(acetonitrile) complex 4 is herein described, since it has not been previously

reported. It is indicative of a very weak CO_2 electrocatalyzed reduction (Table 1, Figure S22), with a value for the catalytic activity $\frac{i_{cat}(CO_2)}{i_p(Ar)}$ of 2.1, that is, clearly below those obtained for

the complexes 1, 2, and 3, which contain 1,2-azole ligands.

Electrocatalysis Voltammetry. The mechanism for the electrocatalytic reduction of CO₂ with complexes containing the "cis-Ru^{II}(bipy)₂" moiety is well established^{1,4} and starts with a one-electron reduction, followed immediately by a second one-electron reductive dehalogenation that affords a five-coordinate species of the type [Ru⁰(bipy)₂L]. This neutral complex is the active species, which initiates the catalytic cycle by coordinating a CO_2 molecule to form the η^1 - CO_2 adduct required to start the reduction process. In our case, the first reduction is always reversible, as indicated above (Figure S5 for 1b, Figures S13 and S14 for 2b, and Figure S20 for 3), and the onset potential of the CO2 reduction always occurs after the second or with the third electron reduction process (see Figure 2 as well as Figures S2, S6, S8, S10, S15, S17, and S21). We have found a precedent in the literature where this situation occurs, ²⁴ which is related to the presence of acidic OH groups near the Ru(II) center. In that case, reductions of the complexes were irreversible due to the reductive deprotonation of the ligands. As the 1,2-azole ligands present in our complexes also contain an acidic proton, a similar process where the third reduction observed in the cyclic voltammograms occurs with a reductive deprotonation might be herein proposed.

A second effect observed was the higher catalytic activity of the aquo complexes compared to those of the chlorido complexes. This is to be expected because of the higher lability of the hard aquo ligand in comparison with that of the softer chlorido ligand when coordinated to a soft metallic center, such as Ru(II). After the reduction observed in the voltammograms, this effect should be even more pronounced, since reduction occurs with a further softening of the metallic center.

A third important feature is the peak of the enhanced current at reduction potentials reached by the complexes, which was ca. -3 V for all them except for 1b and 1c, where the plateau was reached at -2.7 V as -2.6 V (see Figures S2, S6, S8, S10, S15, S17, and S21); thus the overpotential $\eta_{\rm cat}$ parameter improved by 0.3 and 0.4 V, respectively. This is also visibile in Table 2 and is supported by the experiment described in the next paragraph. Finally, the presence of the

Table 2. Faradaic Efficiencies and Turnover Numbers (TON) for All Complexes in Acetonitrile after CPE Experiments with a Reticulated Vitreous Carbon Working Electrode Held at -2.7 V for 2 h

	F	E at -2	.7 V ^a		TON	$TOF^{b}(h^{-1})$	
Catalyst	H ₂	СО	НСООН	СО	НСООН	СО	нсоон
1a	<1%	31%	44%	2.6	5	1.3	2.5
1b	<1%	34%	47%	3	5.1	1.5	2.5
1c	<1%	30%	44%	2.9	5	1.5	2.5
2a	<1%	32%	54%	3.4	6.1	1.7	3.1
2b	<1%	35%	52%	3.8	5.9	1.9	2.9
2c	<1%	29%	48%	3.5	5.1	1.7	2.5
3	<1%	30%	49%	2.8	5.1	1.4	2.5
4	<1%	26%	39%	2.3	4.2	1.2	2.1

^aPotential V vs Fc/Fc⁺. ^bDetermined from CPE.

1,2-azole ligands in the electrocatalytic reduction of CO_2 seems to be a determining factor, possibly helping to stabilize some of the intermediates active in the catalytic cycle. It should be also pointed out that the onset potential of the CO_2 reduction in the bis(acetonitrile) complex 4 occurs after the third electron reduction process (see Figure S22), suggesting that the lower catalytic activity in this complex may occur by a different mechanism.

Controlled potential electrolysis. To further evaluate the catalytic activity of the ruthenium complexes described in this work, we performed controlled potential electrolysis (CPE) studies. CPE was carried out in CH₂CN using a three-electrode setup with a glassy carbon working electrode and at -2.7 V vs the Fc⁺/Fc couple. The gaseous products, H₂ and CO, were then analyzed by sampling the headspace of the electrolysis cell using gas chromatography. The determination of the amount of formic acid was accomplished using ¹H NMR spectroscopy.⁶⁶ The results, which are compiled in Table 2, show that the catalysts are selective toward the reduction of CO₂ over that of protons. Two products were formed from CO₂, formic acid and CO; the former product was produced at higher yields than the latter. The formation of formic acid may be due to the presence of adventitious water present in the experiment, as reported by other groups.⁴ No signals of free 1,2-azole were detected in the ¹H NMR spectra recorded after the CPE experiments, which is an indication of the high stability of the complexes during the catalytic process. Just as was observed in the cyclic voltammetry experiments, the aquo complexes were more active and produced c.a. 20% more product than their chloride counterparts.

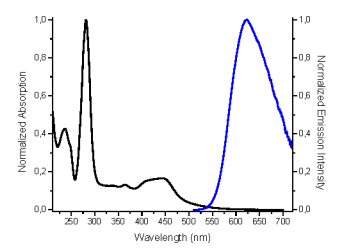
Photophysical Studies. The absorption and emission spectral data for complexes 1 and 2 are summarized in Tables 3 and 4. Complexes 3 and 4 did not show any luminescent

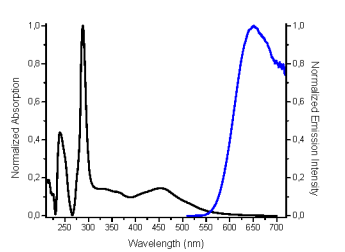
Table 3. Absorption and Emission Data of Complexes in MeCN

	Absorption	Emission		
Complex	λ nm ($\varepsilon \times 10^{-3} \text{ M}^{-1} \text{ cm}^{-1}$)	$\lambda_{\rm em}$ (nm) ($\lambda_{\rm excit}$ = 420 nm)		
1a	237 (19.9), 287 (49.5), 341 (7.3), 477 (7.3)	625		
1b	236 (24.1), 287 (54.9), 338 (8.1), 476 (8.3)	646		
1c	236 (23.5), 287 (55.8), 341 (8.6), 473 (8.5)	640		
2a	237 (18.3), 282 (43.1), 339 (5.4), 364 (5.5), 444 (7.1)	624		
2b	232 (21.8), 281 (48.9), 333 (5.9), 373 (8.1), 411 (9.2), 429 (9.0)	621		
2c	236 (19.4), 283 (43.9), 342 (6.5), 358 (6.4), 455 (6.9)	638		

Table 4. Emission Data of Complexes in Different Solvents

			Emission			
Complex	Solvent	0×10^{-2}	τ (ns)	χ^2	$k_{\rm r} (10^4 { m s}^{-1})$	$k_{\rm nr} {10^4 \atop { m s}^{-1}}$
1a	THF	1.41	46.1	1.01	30.6	2138.6
1b	MeCN	0.15	42.1	1.30	3.6	2371.7
1c	MeCN	0.92	178.5	1.18	5.2	555.1
2a	THF	2.23	37.3	1.08	59.8	2621.2
2b	THF	1.33	64.9	1.05	20.5	1520.3
2c	MeCN	1.01	144.9	1.11	7.0	683.2





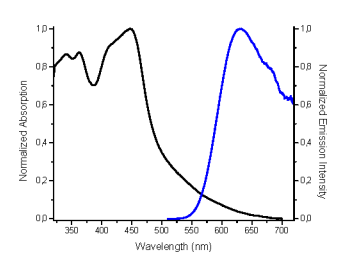


Figure 3. Normalized UV—vis absorption (black) and emission (blue, $\lambda_{ex} = 420$ nm) spectra at 298 K in optically dilute solutions of **2a** in MeCN (left), THF (center), and acetone (right).

Table 5. Photocatalytic Experiments with Ru Complexes (0.1 mM) in a Solvent Mixture of CH₃CN/TEOA (5:1 v/v) with 1.6 mM [Ru(bipy)₃]Cl₂ as the Photosensitizer (PS) and TEOA as the Electron Donor (ED)^aReaction conditions are as follows for all the experiments: irradiation with a >300 nm light for 24 h, light intensity of 150 mW/cm², and 25 °C.

Entry	Catalyst	PS	CO (µmol)	CO (TON)	HCOOH (µmol)	HCOOH (TON)	H_2 (μ mol)
1	1a	$[Ru(bipy)_3]^{2+}$	5.1	21	15	60	2
2	1b	$[Ru(bipy)_3]^{2+}$	4.4	18	16	66	4
3	1c	$[Ru(bipy)_3]^{2+}$	5.8	23	13	56	3
4	2a	$[Ru(bipy)_3]^{2+}$	7.2	28	18	68	3
5	2b	$[Ru(bipy)_3]^{2+}$	5.6	23	17	70	2
6	2c	$[Ru(bipy)_3]^{2+}$	7.6	31	19	76	3
7	3	$[Ru(bipy)_3]^{2+}$	4.5	18	16	66	3
8	4	$[Ru(bipy)_3]^{2+}$	3.2	12	11	48	2
9	1 ^a	-	<1	<2	<1	<1	<1
10	$1^{a,b}$	$[Ru(bipy)_3]^{2+}$	-	-	-	-	-

^aControl experiments ^bTEOA was not added to the mixture.

behavior. The absorption spectral data of the pzH (1a) and dmpzH (1c) chlorido complexes were previously reported by Jude et al., 48 and the indzH (1b) complex was characterized by Fonteles et al. 49 However, we measured all of them again under the same conditions to compare the results with those of the (1,2-azole)-aquo complexes 2. The absorption and emission spectra (those of 2a are shown in Figure 3) as well as the wavelength maxima detected in the different deaerated solvents at 298 K are collected in the Supporting Information (Figure S23). The spectra show absorption profiles similar to those for previously reported complexes of this type. 46,59 All the complexes display intense absorption bands in the 250-300 nm region, which may be attributed to $\pi(L) \to \pi^*(L)$ IL, and lower energy broad bands above 300 nm corresponding to $d\pi(Ru) \rightarrow \pi^*(L)$ MLCT. The low energy bands of all the complexes are blue-shifted when the chlorido ligand is substituted by the aquo ligand. These blue shifts originate from electronic effects induced by the substitution of the anionic electron-donating chlorido ligand by the neutral σ donating aquo ligand.

The emission spectra show one unstructured broad band, which is solvent-dependent (around 20 nm shifts for all the complexes). The intensities in the emission spectra show a dramatic increase in the deaerated solutions compared to those prepared without the exclusion of air, with no variation in the emission maxima (Figure S24). These results, along with luminescent emission lifetimes (see below), are characteristic features of ³MLCT phosphorescent emissions. ^{67,68}

As the solvent does not affect the quantum yields and the luminescent emission lifetimes, the complexes were measured in different solvents depending on their solubility (Table 4). Both are similar to those reported for other bis(bipyridine)-ruthenium(II) complexes.⁶³ The comparison among the quantum yields of (1,2-azole)-aquo complexes 2 with the

(1,2-azole)-chlorido complexes 1 leads to significant variations, showing that complexes 2 have higher quantum yields in all cases. A reviewer pointed out the higher values of the luminescent emission lifetimes for complexes 1c and 2c compared to the rest. Unfortunately, we are unable to find a straightforward explanation for this feature. The radiative and nonradiative rate constants for 1c and 2c are shorter than those for the other complexes, what is also in accordance with the lower values of their quantum yields. The data obtained for all complexes are well-described by single-exponential decays, as indicated by the fact that the quality-of-fit $\chi 2$ values are close to the ideal value of 1 and range from 1.01–1.30.

Photocatalytic Experiments. The complexes herein described are both catalysts for CO2 reduction and luminescent; therefore, we decided to explore their activity as photocatalysts. However, the results of the experiments carried out with these complexes as both the photocatalyst and the photosensitizer were unsatisfactory. Therefore, we decided to explore their photocatalytic activity in the presence of $[Ru(bipy)_3]^{2+}$. The photocatalytic CO_2 reduction experiments were carried out in a CO₂-saturated CH₃CN/TEOA (5:1 v/v) solution containing a mixture of the catalyst and $[Ru(bipy)_3]^{2+}$ as the photosensitizer in a glass vial with a volume of 10 mL under continuous irradiation (light intensity of 150 mW/cm² at 25 °C, λ > 300 nm) (Table 5). To validate the photocatalytic data, various control experiments were carried out under different experimental conditions under irradiation with light. In the absence of $[Ru(bipy)_3]^{2+}$, the catalyst, or the sacrificial electron donor, TEOA, only a trace amount or no amount of product was produced, indicating that all the three components are necessary for efficient CO2 activation. The formic acid produced was quantified using the protocol reported by Kubiak et al.⁶⁹ For all complexes, formic acid production was 2-3 times that of CO formation after 24 h.

Recently, a similar complex, $[Ru(bipy)_2(CO)_2]^{2+}$, was shown to produce formic acid over CO under similar photocatalytic conditions using [Ru(bipy)₃]²⁺ as a photosensitizer. To When a different photosensitizer, [Ir(ppy)₃] (ppy = 2-phenylpyridine), was used, the ratio of products changed to favor CO formation regardless of whether acetonitrile or DMF was used as a solvent. All photocatalysts produced similar amounts of products, where the TON for the production of formic acid ranged from 48 to 76 and the TON for CO formation varied from 12 to 31. It is likely that more formate is produced under these reaction conditions since the presence of traces of water can act as the source of protons. ¹H NMR experiments show that mixing complexes 1, 2, or 3 in a CD₃CN solution with excess TEOA does not deprotonate the 1,2-azole. However, the option that deprotonation by TEOA might occur in the reduced complexes can not be completely discarded, even though the 1,2-azole ligand would be less acidic in these conditions. Similarly to the electrocatalysis results, the aquo complexes are the best photocatalysts under these reaction conditions. It is likely that, for the photocatalysts presented in this work, the reaction conditions can be optimized for the production of either CO or formic acid as demonstrated by Rodrigues et al.;⁷³ thus, we will not speculate on the influence of the ligands toward selectivity.

CONCLUSIONS

A family of the scarcely explored complexes of the type $[Ru^{II}(bipy)_2LX]$, (L = N-donor monodentate ligandf and X = halido or labile ligand) are described (herein L is a 1,2-azole derivative and X is Cl or H2O). Four of them have been crystallographically characterized. The complexes show phosphorescent behavior with quantum yields comparable to those of other ruthenium(II) complexes. The complexes efficiently reduce, both electrochemically and photochemically, CO₂ to CO and formic acid. Formic acid is the major product in the reactions. Among the metal complexes with electrochemical or photochemical activity for CO2 reduction, these a very viable option as they can be easily synthesized and may allow a fine-tuning of the electrochemical, luminescent, and catalytic activity simply by using different 1,2-azoles (or other ligands) or substituting the chlorido or aquo ligand with different donors. Further studies in this direction are currently underway.

■ EXPERIMENTAL SECTION

General Remarks. All manipulations were performed under a N₂ atmosphere following conventional Schlenk techniques. Solvents were purified according to standard procedures. cis-[Ru(bipy)₂Cl₂]⁵² was obtained as previously described by our group. All other reagents were obtained from the usual commercial suppliers and used as received. Infrared spectra were recorded in solid in a Bruker Tensor 27 FTIR spectrometer. Standard abbreviations are used to indicate intensity as follows: w = weak, m = medium, s = strong, and vs = very strong. NMR spectra were recorded on 500 MHz Agilent DD2 and 400 MHz Agilent MR instruments in the Laboratorio de Técnicas Instrumentales (LTI), University of Valladolid, using (CD₃)₂CO or (CD₃)₂SO as solvents at room temperature (rt). ¹H, ¹³C, and ¹⁵N NMR chemical shifts (δ) are reported in parts per million (ppm) and are referenced to either tetramethylsilane (TMS, for ¹H and ¹³C NMR) or to nitromethane (CH3NO2, for 15N NMR) using the residual solvent peak as an internal reference. Coupling constants (J) are reported in Hz. Standard abbreviations are used to indicate multiplicity as follows: s = singlet, d = doublet, ddd = doublet of doublet of doublets, dt=

doublet of triplets, t = triplet, and m = multiplet. The full assignment of the 1H NMR spectra was supported by typical homonuclear $^1H-^1H$ correlations such as COSY, TOCSY, and NOESY experiments, and the assignment of $^{13}C\{^1H\}$ and ^{15}N NMR data was supported by HMBC and HSQC heteronuclear experiments (Figure 4). Elemental analyses were performed on a Thermo Fisher Scientific EA Flash 2000.

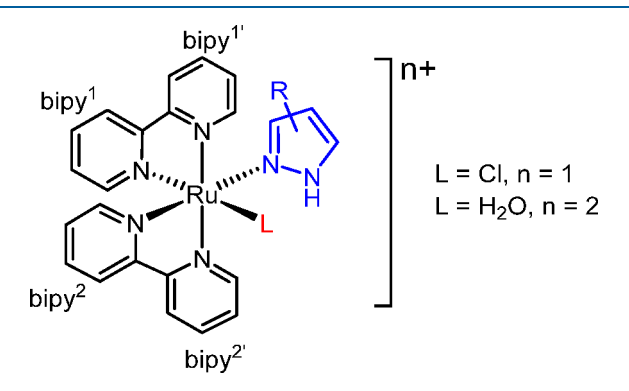


Figure 4. Numbering of bipy for NMR assignment.

cis-[Ru(bipy)₂Cl(pzH)]OTf (1a). This complex was prepared by a modification of the method previously described in the literature. Its synthesis and some spectroscopic data were previously reported.⁴⁸

AgOTf (0.256 g, 1.0 mmol) was added to a mixture of cis-[Ru(bipy)₂Cl₂] (0.520 g, 1.0 mmol) in MeOH (40 mL), and the mixture was stirred at rt for 24 h in the absence of light. The solution was filtered to remove solid AgCl. pzH (0.068 g, 1.0 mmol) was then added, and the mixture was stirred at 40 °C for 24 h. The solvent was then removed in vacuo to give a red solid, which was washed with Et_2O (3 × 5 mL approximately) and dried in vacuo, yielding 0.579 g (87%). ¹H NMR (500 MHz, acetone- d_6): δ 12.78 (s, NH pzH, 1H), 9.99 (d, J = 1.1 Hz, $H^{6'}$ bipy, ¹ 1H), 8.72 (d, J = 8.1 Hz, $H^{3'}$ bipy, ² 1H), 8.69 (d, J = 8.2 Hz, $H^{3'}$ bipy, ¹ 1H), 8.65 (d, J = 8.2 Hz, H^{3} bipy, ¹ 1H), 8.60 (d, J = 8.1 Hz, H^{3} bipy, 1H), 8.27 (d, J = 5.4 Hz, $H^{6'}$ bipy, ² 1H), 8.16 (t, J = 7.9 Hz, $H^{4\prime}$ bipy¹ and $H^{4\prime}$ bipy², 2H), 8.06 (d, J = 4.4Hz, H⁶ bipy¹, 1H), 8.03-7.96 (m, H⁵ pzH and H⁴ bipy¹, 2H), 7.94 (td, J = 7.9, 1.4 Hz, H⁴ bipy², 1H), 7.83 (d, J = 5.1 Hz, H⁶ bipy², 1H), 7.79 (ddd, J = 7.4, 5.7, 1.3 Hz, H⁵ bipy¹, 1H), 7.69 (ddd, J = 7.4, 5.6, 1.3 Hz, H⁵ bipy², 1H), 7.39 (ddd, J = 7.4, 5.7, 1.4 Hz, H⁵ bipy¹, 1H), 7.31 (ddd, J = 7.3, 5.7, 1.3 Hz, H⁵ bipy², 1H), 6.66 (t, J = 1.8 Hz, H³ pzH, 1H), 6.37 (dd, J = 2.3 Hz, H⁴ pzH, 1H). ¹³C NMR (126 MHz, pzH, 1H), 6.37 (dd, f = 2.3 Hz, H pzH, 1H). C NMR (120 MHz, acetone- d_6): δ 160.01 (1C, C^2 bipy¹), 159.02 (1C, C^2 bipy²), 158.31 (1C, C^2 bipy²), 157.98 (1C, C^2 bipy¹), 153.09 (1C, C^6 bipy¹), 153.01 (1C, C^6 bipy¹), 152.17 (1C, C^6 bipy²), 136.08 (1C, C^6 bipy²), 139.75 (1C, C^3 pzH), 136.25 (1C, C^4 bipy²), 136.02 (1C, C^4 bipy¹), 135.88 (1C, C^4 bipy²), 135.58 (1C, C^5 bipy²), 136.02 pzH), 126.79 (1C, C⁵ bipy¹), 126.60 (1C, C⁵' bipy²), 126.37 (1C, C⁵' bipy¹), 125.94 (1C, C⁵ bipy²), 123.72 (1C, C³ bipy¹), 123.31 (1C, C³' bipy²), 123.2 (1C, C³' bipy¹), 123.00 (1C, C³ bipy²), 107.48 (1C, C⁴ pzH). ¹⁵N NMR (51 MHz, acetone- d_6): δ –116.80 (1N, N¹ bipy²), -121.20 (1N, N¹ bipy¹), -121.66 (1N, N² pzH), -124.84 (1N, N¹ bipy²), -127.13 (1N, N¹ bipy¹), -172.33 (1N, N¹ pzH)). IR (solid, cm⁻¹): 3598 w, 3529 w, 3250 m, 3108 w, 3076 w, 2288 w, 2189 w, 2165 w, 2141 w, 2113 w, 2051 w, 1981 w, 1625 w, 1602 m, 1562 w, 1520 w, 1483 w, 1463 s, 1444 s, 1419 s, 1348 w, 1257 vs, 1224 vs, 1148 vs, 1123 vs, 1055 m, 1029 vs, 968 w, 888 w, 857 w, 801 w, 761 vs, 730 vs, 659 m, 635 vs. Anal. Calcd for 1a·CH₃CO C₂₆H₂₃ClF₃N₆O₄RuS: C, 44.03; H, 3.26; N, 11.85; S, 4.52. Found: C, 43.91; H, 3.05; N, 12.10; S, 4.62.

cis-[Ru(bipy)₂Cl(indzH)]OTf (1b). This complex was prepared by a modification of the method previously described in the literature. Its synthesis and some spectroscopic data were previously reported.⁴⁹

To a solution containing [Ru(bipy)₂Cl(OTf)] (1.0 mmol) in MeOH (40 mL), obtained as indicated for 1a, was added indzH (0.118 g, 1.0 mmol), and the mixture was stirred at 50 °C for 24 h.

Work-up as for 1a gave 1b as a red solid, yielding 0.630 g (88%). ¹H NMR (500 MHz, acetone- d_6): δ 12.83 (s, NH indzH, 1H), 9.99 (d, J = 5.6 Hz, $H^{6'}$ bipy¹, 1H), 8.75–8.63 (m, H^3 bipy¹, $H^{3'}$ bipy¹ and $H^{3'}$ bipy², 1H), 8.61 (d, J = 8.2 Hz, H³ bipy², 1H), 8.41 (d, J = 5.5 Hz, H⁶' bipy², 1H), 8.18-8.05 (m, H⁴' bipy², H⁴' bipy¹ and H⁶ bipy¹, 3H), 8.00 (t, J = 7.9 Hz, H⁴ bipy¹, 1H), 7.93 (t, J = 7.9 Hz, H⁴ bipy², 1H), 7.82 (d, J = 5.6 Hz, H^6 bipy², 1H), 7.81–7.71 (m, H^7 indzH, H^5 bipy¹, 1H), 7.62 (t, H⁵' bipy², 1H), 7.57 (d, J = 8.2 Hz, H⁴ indzH, 1H), 7.45-7.35 (m, H³ indzH, H⁶ indzH, and H⁵ bipy¹, 3H), 7.32 (t, H⁵ bipy², 1H), 7.13 (t, J = 7.6 Hz, H⁵ indzH, 1H). ¹³C NMR (126 MHz, acetone- d_6): δ 159.85 (1C, C² bipy¹), 158.71 (1C, C² bipy²), 158.16 (1C, C² bipy²), 157.85 (1C, C bipy), 158.71 (1C, C² bipy²), 158.16 (1C, C² bipy²), 157.91 (1C, C² bipy¹), 153.10 (1C, C² bipy¹), 152.96 (1C, C² bipy¹), 152.28 (1C, C³ bipy²), 152.00 (1C, C³ bipy²), 140.88 (1C, C³ indzH), 136.55 (1C, C⁴ bipy²), 136.22 (1C, C⁴ bipy²), 136.16 (1C, C⁴ bipy²), 136.01 (1C, C³ indzH), 135.89 (1C, C⁴ bipy¹), 127.60 (1C, C⁵ indzH), 127.01 (1C, C⁵ 135.89 (1C, C bipy'), 127.00 (1C, C indzri), 127.01 (1C, C bipy'), 126.69 (1C, C⁵ bipy²), 126.46 (1C, C⁵ bipy'), 126.03 (1C, C³ bipy²), 123.94 (1C, C³ bipy'), 123.82 (1C, C³ a indzri), 123.46 (1C, C³ bipy'), 123.40 (1C, C³ bipy²), 123.06 (1C, C³ bipy'), 121.73 (1C, C⁵ indzri), 119.72 (1C, C⁴ indzri), 119.72 (1C, C⁷ indzri), 15N NMR (51 MHz, acetone- d_6): $\delta - 117.96$ (1N, $N^{1/1}$ bipy²), - 122.63 $(1N, N^{1'} \text{ bipy}^1), -125.19 (1N, N^1 \text{ bipy}^2), -128.08 (1N, N^1 \text{ bipy}^1),$ -132.97 (1N, N² indzH), -195.70 (1N, N¹ indzH). IR (solid, cm⁻¹): 3496 w, 3265 w, 3108 w, 3074 w, 2973 w, 2873 w, 1739 w, 1624 w, 1603 w, 1566 w, 1508 w, 1485 m, 1462 m, 1445 m, 1421 m, 1378 w, 1354 w, 1313 w, 1257 vs, 1234 s, 1221 vs, 1145 s, 1123 m, 1112 m, 1073 w, 1029 vs, 962 w, 901 w, 875 w, 830 w, 802 w, 755 vs, 729 vs, 659 w, 634 vs. Anal. Calcd for C₂₈H₂₂ClF₃N₆O₃RuS: C, 46.96; H, 3.10; N, 12.74; S, 4.48. Found: C, 46.40; H, 3.07; N, 12.42; S, 4.32.

cis-[Ru(bipy)₂Cl(dmpzH)]OTf (1c). This complex was prepared by a modification of the method previously described in the literature. Its synthesis by conventional methods and some spectroscopic data were previously reported.⁴⁸

To a solution containing [Ru(bipy)₂Cl(OTf)] (1.0 mmol) in MeOH (40 mL), obtained as indicated for 1a, was added dmpzH (0.111 g, 1.0 mmol), and the mixture was stirred at 50 °C for 24 h. Work-up as for 1a gave 1c as a red solid, yielding 0.583 g (84%). ¹H NMR (500 MHz, acetone- d_6): δ 12.40 (s, NH dmpzH, 1H), 10.03 (d, $J = 5.6 \text{ Hz}, \text{ H}^{6'} \text{ bipy}^1, 1\text{H}), 8.74 \text{ (d, } J = 8.2 \text{ Hz}, \text{ H}^{3'} \text{ bipy}^2, 1\text{H}), 8.67$ $(d, J = 9.1 \text{ Hz}, H^{3'} \text{ bipy}^1, 1H), 8.60 (d, J = 8.2 \text{ Hz}, H^{3'} \text{ bipy}^1 \text{ and } H^{3'})$ bipy², 2H), 8.56 (d, J = 4.2 Hz, H⁶ bipy², 1H), 8.22–8.13 (m, H⁴ bipy² and H⁴' bipy¹, 2H), 8.11 (d, J = 6.5 Hz, H⁶ bipy¹, 1H), 7.97– 7.89 (m, H⁴ bipy¹ and H⁴ bipy², 2H), 7.82 (ddd, J = 7.6, 5.7, 1.3 Hz, H⁵' bipy¹, 1H), 7.76-7.69 (m, H⁵' bipy² and H⁶ bipy², 2H), 7.33-7.25 (m, H⁵ bipy¹ and H⁵ bipy², 2H), 5.89 (d, J = 2.5 Hz, H⁴ dmpzH, 1H), 2.28 (s, CH₃⁵ dmpzH, 3H), 1.31 (s, CH₃³ dmpzH, 3H). ¹³C NMR (126 MHz, acetone- d_6): δ 160.23 (1C, C^2 bipy¹), 159.09 (1C, C^2 bipy²), 158.33 (1C, C^2 bipy²), 158.33 (1C, C^2 bipy²), 158.23 (1C, C^2 bipy¹), 153.66 (1C, C^6 bipy¹), 153.32 (1C, C^3 dmpzH), 153.08 (1C, C^6 bipy¹), 152.79 (1C, C^6 bipy²), 152.11 (1C, C^6 bipy²), 141.35 (1C, C^6 dmpzH), 136.22 (1C, C⁴ bipy²), 136.10 (2C, C⁴ bipy¹ and C⁴ bipy²), 135.33 (1C, C⁴ bipy¹), 126.61 (1C, C⁵ bipy²), 126.38 (1C, C⁵ bipy¹), 126.26 (1C, C⁵ bipy¹), 126.11 (1C, C⁵ bipy²), 123.60 (1C, C³ bipy²), 123.45 (1C, C³ bipy²), 123.08 (1C, C³ bipy¹), 122.99 (1C, C³ bipy¹), 107.84 (1C, C⁴ dmpzH), 11.83 (1C, CH₃³ dmpzH), 9.78 (1C, CH₃⁵ dmpzH). ¹⁵N NMR (51 MHz, acetone- d_6): δ -117.30 (1N, N^{1} ' bipy²), -121.56 (1N, N^{1} ' bipy¹), -125.19 (1N, N^{1} bipy²), -126.75 (1N, N¹ bipy¹), -163.15 (1N, N² dmpzH), -173.61 (1N, N¹ dmpzH). IR (solid, cm⁻¹): 3302 m, 3078 w, 2287 w, 2051 w, 1981 w, 1602 w, 1570 m, 1461 m, 1444 m, 1420 m, 1373 w, 1255 vs, 1222 s, 1146 s, 1123 m, 1067 w, 1029 vs, 971 w, 895 w, 801 w, 785 w, 761 vs,728 s, 683 w, 658 w, 634 vs. Anal. Calcd for C₂₆H₂₄ClF₃N₆O₃RuS: C, 44.99; H, 3.49; N, 12.11; S, 4.62. Found: C, 44.95; H, 3.46; N, 12.02; S, 4.60.

cis-[Ru(bipy)₂(H₂O)(pzH)](OTf)₂ (2a). AgOTf (0.128 g, 0.5 mmol) and 500 μ L of distillated water were added to a solution of 1a (0.333 g, 0.5 mmol) in Me₂CO (20 mL), and the mixture was stirred at rt for 24 h in the absence of light. The solution was filtered to remove solid AgCl and dried in vacuo. The red residue was crystallized in acetone/Et₂O at -20 °C, giving a red microcrystalline

solid that was decanted, washed with Et_2O (approximately 3 × 5 mL), and dried in vacuo, yielding 0.319 g (80%). ¹H NMR (500 MHz, acetone- d_6): δ 9.51 (d, J = 5.5 Hz, $H^{6\prime}$ bipy¹, 1H), 8.77 (d, J = 8.2 Hz, $H^{3'}$ bipy², 1H), 8.69 (d, J = 5.6 Hz, $H^{6'}$ bipy², 1H), 8.65 (m, $H^{3'}$ bipy¹ and H^3 bipy², 2H), 8.54 (d, J = 8.1 Hz, H^3 bipy¹, 1H), 8.29–8.19 (m, H⁴' bipy² and H⁴' bipy¹, 2H), 8.03-7.96 (m, H⁴ bipy² and H⁶ bipy¹, 2H), 7.96-7.87 (m, H⁴ bipy¹, H⁶ bipy², H⁵' bipy¹ and H⁵ pzH, 4H), 7.78 (t, J = 6.6 Hz, H⁵' bipy², 1H), 7.38-7.29 (m, H⁵ bipy¹, H⁵ bipy² and H³ pzH, 3H), 6.44 (s, H⁴ pzH, 1H). ¹³C NMR (126 MHz, acetone): δ 159.95 (1C, C² bipy¹), 458.91 (1C, C² bipy²), 158.30 (1C, C² bipy²), 157.58 (1C, C² bipy¹), 154.14 (1C, C⁶ bipy¹), 153.24 (1C, C⁶ bipy²), 153.08 (1C, C⁶ bipy²), 151.47 (1C, C⁶ bipy¹), 141.26 (1C, C³ pzH), 137.73 (1C, C⁴ bipy¹), 137.38 (1C, C⁴ bipy²), 137.24 (1C, C⁴ bipy²), 136.16 (1C, C⁴ bipy¹), 132.86 (1C, C⁵ pzH), 127.31 (1C, C⁵ bipy¹), 127.26 (1C, C⁵ bipy²), 126.83 (1C, C⁵ bipy¹), 126.55 (1C, C⁵ bipy²), 123.92 (1C, C³ bipy²), 123.79 (1C, C³ bipy¹), 123.61 (1C, C³' bipy¹), 123.52 (1C, C³ bipy²), 107.47 (1C, C⁴ pzH). ¹⁵N NMR (51 MHz, acetone- d_6): δ –124.77 (1N, N¹ bipy¹), $-126.10 (1N, N^{1} \text{ bipy}^2), -130.38 (1N, N^{1} \text{ bipy}^2), -134.49 (1N, N^{1} \text{ bipy}^1), -153.58 (1N, N^{2} \text{ pzH}), -174.07 (1N, N^{1} \text{ pzH}). IR (solid,$ cm⁻¹): 3251 m, 3113 m, 2324 w, 2164 w, 2113 w, 2051 w, 1981 w, 1605 m, 1529 w, 1486 m, 1467 m, 1426 m, 1358 w, 1314 vs, 1242 vs, 1155 vs, 1128 vs, 1064 w, 1050 m, 1028 vs, 970 m, 950 m, 909 m, 872 w, 759 vs, 730 vs, 661 w, 632 vs, 609 m. Anal. Calcd for 2a·H₂O C₂₅H₂₂F₆N₆O₇RuS₂: C, 36.81; H, 2.97; N, 10.30; S, 7.86. Found: C, 36.77; H, 3.02; N, 9.73; S, 8.13.

cis-[Ru(bipy)₂(H₂O)(indzH)](OTf)₂ (2b). The same procedure as that for 2a was used with 1b (0.358 g, 0.5 mmol) as the starting material, yielding 0.351 g (83%) of 2b as a red microcrystalline solid. ¹H NMR (500 MHz, acetone- d_6): δ 9.55 (d, I = 5.6 Hz, $H^{6'}$ bipy¹, 1H), 8.82-8.76 (m, $H^{6'}$ bipy² and $H^{3'}$ bipy², 2H), 8.66 (d, J=8.2 Hz, H^{3} bipy², 1H), 8.63 (d, J=8.1 Hz, $H^{3'}$ bipy¹, 1H), 8.54 (d, J=8.2 Hz, H^3 bipy¹, 1H), 8.26 (t, J = 8.4 Hz, $H^{4\prime}$ bipy², 1H), 8.20 (t, J = 7.5 Hz, H⁴' bipy¹, 1H), 8.08-7.98 (m, H³ indzH, H⁴ bipy², and H⁶ bipy¹, 3H), 7.98–7.87 (m, H⁴ bipy¹, H⁶ bipy², and H⁵' bipy¹, 3H), 7.73 (t, J = 7.3 Hz, $H^{5'}$ bipy², 1H), 7.66 (d, J = 8.3 Hz, H^{4} indzH, 1H), 7.56 (d, $I = 8.6 \text{ Hz}, \text{ H}^7 \text{ indzH}, \text{ 1H}), 7.43 - 7.34 \text{ (m, H}^6 \text{ indzH}, \text{H}^5 \text{ bipy}^1, \text{ and}$ H^5 bipy², 3H), 7.16 (t, J = 8.0 Hz, H^5 indzH, 1H). ¹³C NMR (126 MHz, acetone): δ 159.83 (1C, C^{2} bipy¹), 158.72 (1C, C^{2} bipy²), 158.20 (1C, C² bipy²), 157.49 (1C, C² bipy¹), 154.20 (1C, C⁶ bipy¹), 153.27 (1C, C⁶ bipy²), 152.94 (1C, C⁶ bipy²), 151.50 (1C, C⁶ bipy¹), 141.79 (1C, C^{7a} indzH), 137.92 (1C, C⁴ bipy²), 137.63 (1C, C⁴ bipy¹), 137.49 (1C, C³ indzH), 137.20 (1C, C⁴ bipy²), 136.44 (1C, C⁴ bipy¹), 128.00 (1C, C⁵ bipy¹), 127.44 (1C, C⁵ bipy¹), 127.32 (1C, C shpy), 128.00 (1C, C shpy), 127.44 (1C, C shpy), 127.32 (1C, C^{5'} bipy²), 127.01 (1C, C⁵ bipy²), 126.65 (1C, C⁶ IndzH), 124.00 (1C, C^{3'} bipy²), 123.91 (1C, C³ bipy¹), 123.68 (1C, C^{3'} bipy¹), 123.58 (1C, C³ bipy²), 123.34 (1C, C^{3a} indzH), 122.00 (1C, C³ indzH), 119.96 (1C, C⁴ indzH), 110.10 (1C, C⁷ indzH). ¹⁵N NMR (51 MHz, acetone- d_6): δ –126.29 (1N, N¹ bipy¹), –126.95 $(1N, N^{1} \text{ bipy}^2), -131.04 (1N, N^{1} \text{ bipy}^2), -135.68 (1N, N^{1} \text{ bipy}^1),$ -135.93 (1N, N² indzH), -197.76 (1N, N¹ indzH). IR (solid, cm⁻¹): 3235 m, 3117 m, 2324 w, 2164 w, 2051 w, 1981 w, 1626 m, 1605 m, 1568 w, 1509 w, 1466 m, 1426 m, 1385 w, 1357 w, 1222 vs, 1162 vs, 1125 vs, 1067 m, 1025 vs, 965 m, 902 w, 854 w, 840 w, 800 w, 763 vs, 729 s, 661 w, 632 vs. Anal. Calcd for **2b**·H₂O C₂₉H₂₄F₆N₆O₇RuS₂: C, 40.23; H, 3.03; N, 9.71; S, 7.41. Found: C, 39.89; H, 2.83; N, 9.46; S,

cis-[Ru(bipy)₂(H₂O)(dmpzH)](OTf)₂ (2c). The same procedure as that for 2a was used with 1c (0.347 g, 0.5 mmol) as the starting material, yielding 0.310 g (78%) of 2c as a red microcrystalline solid. ¹H NMR (500 MHz, acetone- d_6): δ 9.71 (d, J = 5.3 Hz, H⁶′ bipy¹, 1H), 8.83 (m, H⁶′ bipy² and H³′ bipy², 2H), 8.69 (m, H³′ bipy¹ and H³ bipy², 2H), 8.57 (d, J = 8.0 Hz, H³ bipy¹, 1H), 8.29 (td, J = 8.0, 1.4 Hz, H⁴′ bipy², 1H), 8.25 (td, J = 8.0, 1.4 Hz, H⁴′ bipy¹, 1H), 8.09 (d, J = 5.7 Hz, H⁶ bipy¹, 1H), 8.01 (td, J = 8.0, 1.4 Hz, H⁴ bipy², 1H), 7.96–7.86 (m, H⁴ bipy¹, H⁶ bipy², and H⁵′ bipy¹, 4H), 7.82 (ddd, J = 7.4, 5.6, 1.2 Hz, H⁵′ bipy², 1H), 7.34 (ddd, J = 7.4, 5.7, 1.3 Hz, H⁵ bipy², 1H), 7.28 (ddd, J = 7.3, 5.8, 1.3 Hz, H⁵ bipy¹, 1H), 5.97 (s, H⁴ dmpzH, 1H), 2.26 (s, CH₃⁵ dmpzH, 3H), 1.48 (s, CH₃³ dmpzH, 3H). ¹³C NMR (126 MHz, acetone): δ 160.28 (1C, C² bipy¹), 159.09 (1C,

C² bipy²), 158.48 (1C, C²' bipy²), 157.78 (1C, C²' bipy¹), 154.77 (1C, C6 bipy¹), 153.88 (2C, C6' bipy² and C³ dmpzH), 153.51 (1C, C6 bipy²), 152.23 (1C, C6' bipy¹), 143.19 (1C, C⁵ dmpzH), 137.80 (1C, C⁴' bipy²), 137.28 (2C, C⁴' bipy¹ and C⁴ bipy²), 135.94 (1C, C⁴ bipy¹), 127.25 (1C, C⁵' bipy²), 127.04 (1C, C⁵' bipy¹), 126.59 (1C, C⁵ bipy²), 126.17 (1C, C⁵ bipy¹), 124.09 (1C, C³' bipy²), 123.64 (1C, C³' bipy¹), 123.59 (1C, C³ bipy¹), 123.48 (1C, C³ bipy²), 108.18 (1C, C⁴ dmpzH), 12.56 (1C, CH₃³ dmpzH), 9.89 (1C, CH₃⁵ dmpzH). ¹⁵N NMR (51 MHz, acetone- d_6): δ −124.96 (1N, N¹' bipy²), −126.46 (1N, N¹' bipy²), −130.52 (1N, N¹ bipy²), −132.89 (1N, N¹ bipy¹), −164.13 (1N, N² dmpzH), −180.07 (1N, N¹ dmpzH). IR (solid, cm⁻¹): 3340 m, 3116 w, 3084 w, 2324 w, 2164 w, 2051 w, 1981 w, 1605 m, 1574 m, 1486 w, 1466 m, 1447 m, 1425 m, 1382 w, 1251 vs, 1150 vs, 1029 vs, 799 w, 787 m, 761 s, 729 s, 660 w, 631 vs. Anal. Calcd for 2c·H2O C₂¬H₂₆F₆N₆O¬RuS₂: C, 38.44; H, 3.35; N, 9.96; S, 7.60. Found: C, 38.26; H, 3.25; N, 9.35; S, 8.09.

cis-[Ru(bipy)2(indzH)2](PF6)2 (3). A mixture of cis-[Ru- $(bipy)_2Cl_2]\cdot 2H_2O$ (0.107 g, 0.2 mmol), indzH (0.052 g, 0.44 mmol), and H₂O (10 mL) was refluxed for 2.30 h. To the mixture was added NH₄PF₆ (0.326 g, 2 mmol), and an orange precipitate appeared. The precipitate was filtered off, washed with Et₂O (approximately 3 × 5 mL), and dried, yielding 0.167 g, 84%. ¹H NMR ((CD₃)₂SO, rt): δ 13.10 (s, H¹ indzH, 2H), 9.23 (d, J = 7 Hz, H⁵ indzH, 2H), 8.62 (d, H³ indzH, 2H), 8.56 (d, J = 8 Hz, H⁶ bipy, 2H), 8.19 (m, H⁷ indzH and H⁶' bipy, 4H), 8.00 (m, H³' bipy, 2H), 7.92 (d, H³ bipy, 2H), 7.87 (m, H⁴ indzH, 2H), 7.66 (d, J = 7 Hz, H⁶ indzH, 2H), 7.49 (m, H⁵ bipy, 2H), 7.38 (m, H⁴ and H⁴⁷ bipy, 4H), 7.14 (m, H⁵' bipy, 2H). 13 C { 1 H} RMN ((CD₃)₂SO, rt): δ 157.6 (2C, $C^{2\prime}$ bipy), 157.03 (2C, C^{2} bipy), 156.9 (2C, C^{7a} indzH), 153.8 (2C, C⁵ indzH), 152.9 (2C, C⁶ bipy), 142.3 (2C, C^{3a} indzH), 138.7 (2C, C⁷ indzH), 138.4 (2C, C⁶ bipy), 138.1 (2C, C⁴ bipy), 128.2 bipy), 127.9 (2C, C⁵ bipy), 127.8 (2C, C⁶ indzH), 124.2 (2C, C⁵ bipy), 123.3 (2C, C³ indzH), 122.2 (2C, C³ bipy), 120.5 (2C, C⁴ indzH), 110.3 (2C, C3' bipy). IR (cm-1): 3642 w, 3573 w, 3431 w, 3126 w, 2323 w, 2163 w, 2139 w, 2111 w, 2050 w, 1980 w, 1938 w, 1627 m, 1603 m, 1510 w, 1466 m, 1444 s, 1423 m, 1385 w, 1359 s, 1326 w, 1313 w, 1274 m, 1244 w, 1223 w, 1153 w, 1129 w, 1076 w, 1026 w, 1004 w, 967 w, 942 w, 902 w, 826 vs, 758 vs, 731 vs, 660 w, 617 w. Anal. Calcd for 3.4MeCN, C₄₂H₄₀F₁₂N₁₂P₂Ru: C, 45.23; H, 3.40; N, 15.61. Found: C, 45.69; H, 3.65; N, 15.23.

Photophysical Experiments. The solvents for spectroscopic studies were of spectroscopic grade and used as received. Ultravioletvisible (UV-vis) and fluorescence spectra were recorded in optically dilute solutions (from 1×10^{-5} to 5×10^{-5} M) at room temperature with a quartz cuvette (1 × 1 cm) using Hitachi U-3900 and F-7000 Hitachi Fluorescence spectrophotometers, respectively. Fluorescence decay lifetimes were measured in deaerated solvents using a timecorrelated single-photon counting instrument (FLS980 Series, Edinburgh instruments) with a 405 nm pulsed LED (Edinburgh instruments, EPL-510) light source with 50-500 ns. The absolute fluorescence quantum yields in each solvent were measured using the integrating sphere accessory with a FLS980 Series Edinburgh instrument, wherein the solvent was used as a reference. χ^2 is a stadistic parameter that accounts for the quality of fit between the observed and the model exponential decays (ideal value of 1). Tail fits and numerical reconvolution were obtained by using the FAST software package (Edinburgh Instruments).

Electrochemical Experiments. Electrochemical measurements were carried out with a Dropsens μ Stat 400 (range from -4 to +4 V, DropView 8400 ver. 2.2 software), Dropsens Stat 300 (range from -2 to +2 V), or PalmSens 3 potentiostat (range from -5 to +5 V, PSTrace4 ver. 4.4.2 software). Unless otherwise stated, CVs were scanned at 200 mV/s, in acetonitrile (5 mL) with a 0.1 M n-Bu₄PF₆ supporting electrolyte, purging with Ar or CO₂ at room temperature through a PTFE tubing. Working electrodes were made of glassy carbon (3 mm diameter). The auxiliary electrode was a platinum wire. The reference electrodes used were either Ag/AgCl (3 M NaCl) MF-2052 BASi (separated from the bulk solution by a "thirsty" Vycor frit) or a silver wire pseudoreference electrode. Ferrocene was added at the end of the experiments. The observed ferrocenium/ferrocene couple

was $E_{1/2}=0.443\pm0.005~{\rm V}$ vs Ag/AgCl. Potential values measured with the Ag wire have plenty of uncertainty, and measurements must be carried out with the Ag/AgCl (3 M NaCl) electrode at the end of the experiment.

The solubility of saturated CO_2 in acetonitrile has been reported to be 0.28 M at 25 °C. 71,72 Changing the atmosphere from pure Ar to pure CO_2 or vice versa required bubbling with the new gas for not less than 5 min. Lasting such time, the CVs obtained were the same than those obtained in the first scan under a specific atmosphere. Bubbling was continued during the interim between scans. During scan time, the PTFE was raised and kept above the surface of the solution to avoid agitation.

Controlled Potential Electrolysis. Controlled potential electrolysis (CPE) studies of the complexes (1 mM) were carried out in CH₃CN with 0.1 M TBAPF₆ as the electrolyte and at $-2.7~\rm V$ vs the Fc $^+$ /Fc couple for 2 h using a model CHI6012D electrochemical workstation. CPE studies were performed in a specialized three-compartment cell with a three-electrode setup consisting of a glassy carbon working electrode, a Ag/AgNO₃ reference electrode, and a platinum wire counter electrode. The solution was saturated with CO₂ (that had been dried by passing it through 5 Å molecular sieves) for 30 min, after which it was made airtight. Then, CPE was initiated.

Product analysis was accomplished according to the nature of the product, i.e., gas or liquid. The gaseous products were analyzed by sampling the headspace of the electrolysis cell using a gastight Hamilton 1001 SL SYR syringe at the conclusion of the electrochemical runs. The analysis was achieved by a Shimadzu GC2014 gas chromatograph equipped with a 60/80 CARBOXEN-1000 15' × 1/8" SS (2.1 mm I.D.) column. For the gaseous sample analysis, a 0.5 mL sample of the gas was injected via the on-column injector by the gastight Hamilton syringe. The carrier gas used was helium. The determination of the amount of formic acid was accomplished using ¹H NMR spectroscopy by a previously reported method. ⁶⁶ Briefly, a calibration curve for formic acid was prepared using an internal standard of dimethyl sulfone in a solvent of D2O to quantify the amount of formic acid in the bulk electrolysis samples. Thereafter, 150 μL of the bulk electrolysis sample was extracted and subsequently mixed with 600 μ L of dimethyl sulfone in a solvent of D₂O. The mixture was then sonicated for 1 min, 400 µL of the mixture was placed in an NMR tube, and ¹H NMR spectra were subsequently recorded. The integration value(s) for the peak at 8.5 ppm was recorded and, with reference to the calibration curve previously established, the amount of formic acid generated in each sample was quantified.

Photocatalysis Procedure. A 20 mL vial containing 0.1 mM catalyst and 1.6 mM $[Ru(bipy)_3]^{2+}$ was added a solvent mixture of $CH_3CN/TEOA$ (5:1 v/v) to afford a total volume of 10 mL. Subsequently, the vial was sealed with a rubber septum, and the solution was bubbled with CO_2 for 20 min. The CO_2 -saturated solution was thereafter irradiated with a 150W EKE Kramer scientific corporation modulamp, a light source with a UV cut-off filter (>300 nm). After the conclusion of the photochemical run, the head space was sampled using a gastight Hamilton 1001 SL SYR syringe. The head space gas analysis was then accomplished using a SHIMADZU GC2014 gas chromatograph equipped with a 60/80 CARBOXEN-1000 15' x1/8" SS (2.1 mm I.D.) column.

Crystal Structure Determination for Compounds 1a, 1b, 2b, and 2c. Crystals were grown either in concentrated solutions of the complexes in methanol (for 1a and 1b) at -20 °C or by the slow diffusion of Et₂O into concentrated solutions of the complexes in acetone (for 2b and 2c) at -20 °C. Relevant crystallographic details can be found in 2031192-2031195. A crystal was attached to a glass fiber and transferred to an Agilent SuperNova diffractometer fitted with an Atlas CCD detector. The crystals were kept at 293(2) K during data collection. Using Olex2, 73 the structures were solved with the ShelXT⁷⁴ structure solution program. Then, the structures were refined with the ShelXL⁷⁵ refinement package using least-squares minimization. All non-hydrogen atoms were refined anisotropically. Hydrogen atoms were set in calculated positions and refined as riding atoms with a common thermal parameter. All graphics were made

with Olex2, and the distances and angles of hydrogen bonds were calculated with PARST^{76,77} (normalized values).^{78,79}

ASSOCIATED CONTENT

Supporting Information

The Supporting Information is available free of charge at https://pubs.acs.org/doi/10.1021/acs.inorgchem.0c02716.

Cyclic voltammograms of complexes 1–4, normalized UV–vis absorption and emission spectra of 1 and 2, emission spectra of 1c and 2c in aerated and deaerated MeCN, photocatalytic experiments, and ¹H NMR spectrum of the photochemical solution of 1c(PDF)

Accession Codes

CCDC 2031192–2031195 contain the supplementary crystallographic data for this paper. These data can be obtained free of charge via www.ccdc.cam.ac.uk/data_request/cif, or by emailing data_request/cif, or by contacting The Cambridge Crystallographic Data Centre, 12 Union Road, Cambridge CB2 1EZ, UK; fax: +44 1223 336033.

AUTHOR INFORMATION

Corresponding Author

Fernando Villafañe — GIR MIOMeT-IU Cinquima-Química Inorgánica, Facultad de Ciencias, Universidad de Valladolid-Campus Miguel Delibes, 47011 Valladolid, Spain; orcid.org/0000-0002-3230-3802; Email: fernando.villafane@uva.es

Authors

Elena Cuéllar – GIR MIOMeT-IU Cinquima-Química Inorgánica, Facultad de Ciencias, Universidad de Valladolid–Campus Miguel Delibes, 47011 Valladolid, Spain

Laura Pastor – GIR MIOMeT-IU Cinquima-Química Inorgánica, Facultad de Ciencias, Universidad de Valladolid–Campus Miguel Delibes, 47011 Valladolid, Spain

Gabriel García-Herbosa — Departamento de Química, Facultad de Ciencias, Universidad de Burgos, 09001 Burgos, Spain; o orcid.org/0000-0002-2863-1272

John Nganga – Department of Chemistry, University of Connecticut, Storrs, Connecticut 06269, United States

Alfredo M. Angeles-Boza — Department of Chemistry, University of Connecticut, Storrs, Connecticut 06269, United States; Occid.org/0000-0002-5560-4405

Alberto Diez-Varga – Departamento de Química, Facultad de Ciencias, Universidad de Burgos, 09001 Burgos, Spain

Tomás Torroba — Departamento de Química, Facultad de Ciencias, Universidad de Burgos, 09001 Burgos, Spain;
o orcid.org/0000-0002-5018-4173

Jose M. Martín-Alvarez – GIR MIOMeT-IU Cinquima-Química Inorgánica, Facultad de Ciencias, Universidad de Valladolid-Campus Miguel Delibes, 47011 Valladolid, Spain; orcid.org/0000-0002-6969-0703

Daniel Miguel — GIR MIOMeT-IU Cinquima-Química Inorgánica, Facultad de Ciencias, Universidad de Valladolid-Campus Miguel Delibes, 47011 Valladolid, Spain; orcid.org/0000-0003-0650-3058

Complete contact information is available at: https://pubs.acs.org/10.1021/acs.inorgchem.0c02716

Author Contributions

The manuscript was written through contributions of all authors. All authors have given approval to the final version of the manuscript.

Notes

The authors declare no competing financial interest.

ACKNOWLEDGMENTS

This research was supported by the Junta de Castilla y León (ref. VA130618). E.C. thanks the UVa for her grant. The authors in Valladolid gratefully acknowledge financial support from the Spanish MINECO, Spain (PGC2018-099470-B-I00) and Junta de Castilla y León (VA130618), and the authors in Burgos gratefully acknowledge financial support from the Junta de Castilla y León, Consejería de Educación y Cultura and Fondo Social Europeo (Project BU263P18). A.M.A.-B. is grateful for support from the National Science Foundation CAREER Grant (CHE-1652606).

REFERENCES

- (1) Takeda, H.; Ishitani, O. Development of Efficient Photocatalytic Systems for CO₂ Reduction Using Mononuclear and Multinuclear Metal Complexes Based on Mechanistic Studies. *Coord. Chem. Rev.* **2010**, 254 (3–4), 346–354.
- (2) Qiao, J.; Liu, Y.; Hong, F.; Zhang, J. A Review of Catalysts for the Electroreduction of Carbon Dioxide to Produce Low-Carbon Fuels. *Chem. Soc. Rev.* **2014**, 43 (2), 631–675.
- (3) Elgrishi, N.; Chambers, M. B.; Wang, X.; Fontecave, M. Molecular Polypyridine-Based Metal Complexes as Catalysts for the Reduction of CO₂. *Chem. Soc. Rev.* **2017**, *46* (3), 761–796.
- (4) Francke, R.; Schille, B.; Roemelt, M. Homogeneously Catalyzed Electroreduction of Carbon Dioxide—Methods, Mechanisms, and Catalysts. *Chem. Rev.* **2018**, *118* (9), 4631–4701.
- (5) Kuramochi, Y.; Ishitani, O.; Ishida, H. Reaction Mechanisms of Catalytic Photochemical CO₂ Reduction Using Re(I) and Ru(II) Complexes. *Coord. Chem. Rev.* **2018**, *373*, 333–356.
- (6) Jiang, C.; Nichols, A. W.; Machan, C. W. A Look at Periodic Trends in d-Block Molecular Electrocatalysts for CO₂ Reduction. *Dalton Trans.* **2019**, 48 (26), 9454–9468.
- (7) Luo, Y.-H.; Dong, L.-Z.; Liu, J.; Li, S.-L.; Lan, Y.-Q. From Molecular Metal Complex to Metal-Organic Framework: The $\rm CO_2$ Reduction Photocatalysts with Clear and Tunable Structure. *Coord. Chem. Rev.* **2019**, 390, 86–126.
- (8) Yamazaki, Y.; Takeda, H.; Ishitani, O. Photocatalytic Reduction of CO₂ Using Metal Complexes. *J. Photochem. Photobiol., C* **2015**, 25, 106–137.
- (9) Ishida, H.; Tanaka, K.; Tanaka, T. Electrochemical CO_2 Reduction Catalyzed by $[Ru(bpy)_2(CO)_2]^{2+}$ and $[Ru(bpy)_2(CO)-Cl]^+$. The Effect of pH on the Formation of CO and HCOO $^-$. Organometallics 1987, 6 (1), 181–186.
- (10) Voyame, P.; Toghill, K. E.; Méndez, M. A.; Girault, H. H. Photoreduction of CO₂ Using [Ru(bpy)₂(CO)L]ⁿ⁺² Catalysts in Biphasic Solution/Supercritical CO₂ Systems. *Inorg. Chem.* **2013**, 52 (19), 10949–10957.
- (11) Ishida, H.; Tanaka, H.; Tanaka, K.; Tanaka, T. Electrochemical Reaction of CO_2 with Me_2NH to Afford N, N -Dimethylformamide, Catalyzed by $[Ru(bpy)_2(CO)_2]^{2+}$ (Bpy = 2,2'-Bipyridine). *Chem. Lett.* **1987**, *16* (4), 597–600.
- (12) Ishida, H.; Tanaka, H.; Tanaka, K.; Tanaka, T. Selective Formation of HCOO⁻ in the Electrochemical CO₂ Reduction Catalysed by $[Ru(bpy)_2(CO)_2]^{2+}$ (Bpy = 2,2'-Bipyridine). *J. Chem. Soc., Chem. Commun.* 1987, No. 2, 131–132.
- (13) Tanaka, K.; Morimoto, M.; Tanaka, T. The Water Gas Shift Reaction Catalyzed by Ruthenium Carbonyl Complexes. *Chem. Lett.* **1983**, *12* (6), 901–904.
- (14) Pugh, J. R.; Bruce, M. R. M.; Sullivan, B. P.; Meyer, T. J. Formation of a Metal-Hydride Bond and the Insertion of CO₂. Key

- Steps in the Electrocatalytic Reduction of Carbon Dioxide to Formate Anion. *Inorg. Chem.* **1991**, *30* (1), 86–91.
- (15) Sullivan, B. P.; Meyer, T. J. Photoinduced Irreversible Insertion of CO_2 into a Metal-Hydride Bond. J. Chem. Soc., Chem. Commun. 1984, 18, 1244–1245.
- (16) Sullivan, B. P.; Caspar, J. V.; Meyer, T. J.; Johnson, S. Hydrido Carbonyl Complexes of Osmium(II) and Ruthenium(II) Containing Polypyridyl Ligands. *Organometallics* **1984**, 3 (8), 1241–1251.
- (17) Hawecker, J.; Lehn, J.-M.; Ziessel, R. Photochemical and Electrochemical Reduction of Carbon Dioxide to Carbon Monoxide Mediated by (2,2'-Bipyridine)Tricarbonylchlororhenium(I) and Related Complexes as Homogeneous Catalysts. *Helv. Chim. Acta* 1986, 69 (8), 1990–2012.
- (18) Lehn, J.-M.; Ziessel, R. Photochemical Reduction of Carbon Dioxide to Formate Catalyzed by 2,2'-Bipyridine- or 1,10-Phenanthroline-Ruthenium(II) Complexes. *J. Organomet. Chem.* **1990**, 382 (1–2), 157–173.
- (19) Sampaio, R. N.; Grills, D. C.; Polyansky, D. E.; Szalda, D. J.; Fujita, E. Unexpected Roles of Triethanolamine in the Photochemical Reduction of CO₂ to Formate by Ruthenium Complexes. *J. Am. Chem. Soc.* **2020**, *142* (5), 2413–2428.
- (20) Kuramochi, Y.; Kamiya, M.; Ishida, H. Photocatalytic CO₂ Reduction in N, N -Dimethylacetamide/Water as an Alternative Solvent System. *Inorg. Chem.* **2014**, *53* (7), 3326–3332.
- (21) Nagao, H.; Mizukawa, T.; Tanaka, K. Carbon-Carbon Bond Formation in the Electrochemical Reduction of Carbon Dioxide Catalyzed by a Ruthenium Complex. *Inorg. Chem.* **1994**, 33 (15), 3415–3420.
- (22) Chen, Z.; Chen, C.; Weinberg, D. R.; Kang, P.; Concepcion, J. J.; Harrison, D. P.; Brookhart, M. S.; Meyer, T. J. Electrocatalytic Reduction of CO_2 to CO by Polypyridyl Ruthenium Complexes. *Chem. Commun.* **2011**, 47 (47), 12607–12609.
- (23) Chen, Z.; Kang, P.; Zhang, M. T.; Meyer, T. J. Making Syngas Electrocatalytically Using a Polypyridyl Ruthenium Catalyst. *Chem. Commun.* **2014**, *50* (3), 335–337.
- (24) Duan, L.; Manbeck, G. F.; Kowalczyk, M.; Szalda, D. J.; Muckerman, J. T.; Himeda, Y.; Fujita, E. Noninnocent Proton-Responsive Ligand Facilitates Reductive Deprotonation and Hinders CO₂ Reduction Catalysis in [Ru(tpy)(6DHBP)(NCCH₃)]²⁺ (6DHBP = 6,6'-(OH)₂bpy). *Inorg. Chem.* **2016**, 55 (9), 4582–4594.
- (25) Johnson, B. A.; Maji, S.; Agarwala, H.; White, T. A.; Mijangos, E.; Ott, S. Activating a Low Overpotential CO₂ Reduction Mechanism by a Strategic Ligand Modification on a Ruthenium Polypyridyl Catalyst. *Angew. Chem., Int. Ed.* **2016**, *55* (5), 1825–1829.
- (26) Johnson, B. A.; Agarwala, H.; White, T. A.; Mijangos, E.; Maji, S.; Ott, S. Judicious Ligand Design in Ruthenium Polypyridyl $\rm CO_2$ Reduction Catalysts to Enhance Reactivity by Steric and Electronic Effects. *Chem. Eur. J.* **2016**, 22 (42), 14870–14880.
- (27) White, T. A.; Maji, S.; Ott, S. Mechanistic Insights into Electrocatalytic CO₂ Reduction within [Ru^{II}(tpy)(NN)X]ⁿ⁺ Architectures. *Dalton Trans.* **2014**, *43* (40), 15028–15037.
- (28) Schneider, T. W.; Hren, M. T.; Ertem, M. Z.; Angeles-Boza, A. M. $[Ru_{II}(tpy)(bpy)Cl]^+$ -Catalyzed Reduction of Carbon Dioxide. Mechanistic Insights by Carbon-13 Kinetic Isotope Effects. *Chem. Commun.* **2018**, 54 (61), 8518–8521.
- (29) Lee, S. K.; Kondo, M.; Nakamura, G.; Okamura, M.; Masaoka, S. Low-Overpotential CO₂ Reduction by a Phosphine-Substituted Ru(II) Polypyridyl Complex. *Chem. Commun.* **2018**, 54 (50), 6915–6018
- (30) Lee, S. K.; Kondo, M.; Okamura, M.; Enomoto, T.; Nakamura, G.; Masaoka, S. Function-Integrated Ru Catalyst for Photochemical CO₂ Reduction. *J. Am. Chem. Soc.* **2018**, *140* (49), 16899–16903.
- (31) Gonell, S.; Massey, M. D.; Moseley, I. P.; Schauer, C. K.; Muckerman, J. T.; Miller, A. J. M. The Trans Effect in Electrocatalytic CO₂ Reduction: Mechanistic Studies of Asymmetric Ruthenium Pyridyl-Carbene Catalysts. *J. Am. Chem. Soc.* **2019**, *141* (16), 6658–6671.
- (32) Huang, J.; Chen, J.; Gao, H.; Chen, L. Kinetic Aspects for the Reduction of CO₂ and CS₂ with Mixed-Ligand Ruthenium(II)

- Hydride Complexes Containing Phosphine and Bipyridine. *Inorg. Chem.* **2014**, *53* (18), 9570–9580.
- (33) Vos, J. G. Excited-State Acid-Base Properties of Inorganic Compounds. *Polyhedron* **1992**, *11* (18), 2285–2299.
- (34) Rommel, S. A.; Sorsche, D.; Fleischmann, M.; Rau, S. Optical Sensing of Anions via Supramolecular Recognition with Biimidazole Complexes. *Chem. Eur. J.* **2017**, 23 (72), 18101–18119.
- (35) Meng, T.-T.; Wang, H.; Zheng, Z.-B.; Wang, K.-Z. pH-Switchable "Off-On-Off" Near-Infrared Luminescence Based on a Dinuclear Ruthenium(II) Complex. *Inorg. Chem.* **2017**, *56* (9), 4775–4779
- (36) Viere, E. J.; Kuhn, A. E.; Roeder, M. H.; Piro, N. A.; Kassel, W. S.; Dudley, T. J.; Paul, J. J. Spectroelectrochemical Studies of a Ruthenium Complex Containing the pH Sensitive 4,4'-Dihydroxy-2,2'-Bipyridine Ligand. *Dalton Trans.* 2018, 47 (12), 4149–4161.
- (37) Brown, R. T.; Fletcher, N. C.; Danos, L.; Halcovitch, N. R. A Tripodal Ruthenium(II) Polypyridyl Complex with pH Controlled Emissive Quenching. *Eur. J. Inorg. Chem.* **2019**, 2019 (1), 110–117.
- (38) Zhang, Z.-H.; He, P.; Kang, S.-R.; Liu, C.; Yi, X.-Y. Reversible Pyrrole-Based Proton Storage/Release in Ruthenium(II) Complexes. *Chem. Commun.* **2019**, *55* (97), 14594–14597.
- (39) Swords, W. B.; Li, G.; Meyer, G. J. Iodide Ion Pairing with Highly Charged Ruthenium Polypyridyl Cations in CH₃CN. *Inorg. Chem.* **2015**, *54* (9), 4512–4519.
- (40) Troian-Gautier, L.; Beauvilliers, E. E.; Swords, W. B.; Meyer, G. J. Redox Active Ion-Paired Excited States Undergo Dynamic Electron Transfer. *J. Am. Chem. Soc.* **2016**, *138* (51), 16815–16826.
- (41) Ghosh, T. K.; Chakraborty, S.; Chowdhury, B.; Ghosh, P. Bis-Heteroleptic Ruthenium(II) Complex of Pendant Urea Functionalized Pyridyl Triazole and Phenathroline for Recognition, Sensing, and Extraction of Oxyanions. *Inorg. Chem.* **2017**, *56* (9), 5371–5382.
- (42) Pannwitz, A.; Poirier, S.; Bélanger-Desmarais, N.; Prescimone, A.; Wenger, O. S.; Reber, C. Controlling Second Coordination Sphere Effects in Luminescent Ruthenium Complexes by Means of External Pressure. *Chem. Eur. J.* **2018**, 24 (31), 7830–7833.
- (43) Sorsche, D.; Rommel, S. A.; Rau, S. Functional Dimming of Pincer-Shaped Bibenzimidazole-Ruthenium(II) Complexes with Improved Anion-Sensitive Luminescence. *Eur. J. Inorg. Chem.* **2016**, 2016 (10), 1503–1513.
- (44) Han, M.-J.; Chen, Y.-M.; Wang, K.-Z. Ruthenium(II) Complexes of 6-Hydroxydipyrido[3,2-a:2',3'-c]Phenazine: Self-Association, and Concentration-Dependent Acid-Base and DNA-Binding Properties. *New J. Chem.* **2008**, 32 (6), 970.
- (45) Zheng, Z.-B.; Kang, S.-Y.; Yi, X.; Zhang, N.; Wang, K.-Z. Off-on-off pH Luminescence Switching and DNA Binding Properties of a Free Terpyridine-Appended Ruthenium Complex. *J. Inorg. Biochem.* **2014**, *141*, 70–78.
- (46) Sullivan, B. P.; Salmon, D. J.; Meyer, T. J.; Peedin, J. Monomeric and Dimeric Pyrazole and Pyrazolyl Complexes of Ruthenium. *Inorg. Chem.* **1979**, *18* (12), 3369–3374.
- (47) Hirahara, M.; Nakano, H.; Uchida, K.; Yamamoto, R.; Umemura, Y. Intramolecular Hydrogen Bonding: A Key Factor Controlling the Photosubstitution of Ruthenium Complexes. *Inorg. Chem.* **2020**, *59*, 11273–11286.
- (48) Jude, H.; Rein, F. N.; Chen, W.; Scott, B. L.; Dattelbaum, D. M.; Rocha, R. C. Pyrazole and Pyrazolyl Complexes of Cis-Bis(2,2′-Bipyridine)- Chlororuthenium(II): Synthesis, Structural and Electronic Characterization, and Acid-Base Chemistry. *Eur. J. Inorg. Chem.* **2009**, 2009 (5), 683–690.
- (49) Sá, D. S.; Fernandes, A. F.; Silva, C. D. S.; Costa, P. P. C.; Fonteles, M. C.; Nascimento, N. R. F.; Lopes, L. G. F.; Sousa, E. H. S. Non-Nitric Oxide Based Metallovasodilators: Synthesis, Reactivity and Biological Studies. *Dalton Trans.* **2015**, *44* (30), 13633–13640.
- (50) Arroyo, M.; Miguel, D.; Villafañe, F.; Nieto, S.; Pérez, J.; Riera, L. Rhenium-Mediated Coupling of Acetonitrile and Pyrazoles. New Molecular Clefts for Anion Binding. *Inorg. Chem.* **2006**, *45* (17), 7018–7026.
- (51) Gómez-Iglesias, P.; Guyon, F.; Khatyr, A.; Ulrich, G.; Knorr, M.; Martín-Alvarez, J. M.; Miguel, D.; Villafañe, F. Luminescent

- Rhenium(I) Tricarbonyl Complexes with Pyrazolylamidino Ligands: Photophysical, Electrochemical, and Computational Studies. *Dalton Trans.* **2015**, 44 (40), 17516–17528.
- (52) Merillas, B.; Cuéllar, E.; Diez-Varga, A.; Asensio-Bartolomé, M.; García-Herbosa, G.; Torroba, T.; Martín-Alvarez, J. M.; Miguel, D.; Villafañe, F. Whole Microwave Syntheses of Pyridylpyrazole and of Re and Ru Luminescent Pyridylpyrazole Complexes. *Inorg. Chim. Acta* **2019**, 484, 1–7.
- (53) Merillas, B.; Cuéllar, E.; Diez-Varga, A.; Torroba, T.; García-Herbosa, G.; Fernández, S.; Lloret-Fillol, J.; Martín-Alvarez, J. M.; Miguel, D.; Villafañe, F. Luminescent Rhenium(I)Tricarbonyl Complexes Containing Different Pyrazoles and Their Successive Deprotonation Products: CO₂ Reduction Electrocatalysts. *Inorg. Chem.* 2020, 59 (15), 11152–11165.
- (54) Kollipara, M. R.; Sarkhel, P.; Chakraborty, S.; Lalrempuia, R. Synthesis, Characterization and Molecular Structure of a New (η^6 -p-Cymene) Ruthenium(II) Amidine Complex, [(η^6 -p-Cymene)Ru{NH = C(Me)3,5-Dmpz}(3,5-Hdmpz)](BF₄)₂·H2O. *J. Coord. Chem.* **2003**, 56 (12), 1085–1091.
- (55) Schlapp-Hackl, I.; Hassenrück, C.; Wurst, K.; Kopacka, H.; Müller, T.; Winter, R. F.; Bildstein, B. Metallo-Scorpionates: First Generation of Trimetallic, Homoleptic [Ru]-M-[Ru] Complexes (M = Fe, Co, Ni, Cu). Eur. J. Inorg. Chem. 2018, 2018 (40), 4434–4441. (56) Gritzner, G.; Kuta, J. Recommendations on Reporting Electrode Potentials in Nonaqueous Solvents (Recommendations
- (57) Rapp, T. L.; Phillips, S. R.; Dmochowski, I. J. Kinetics and Photochemistry of Ruthenium Bisbipyridine Diacetonitrile Complexes: An Interdisciplinary Inorganic and Physical Chemistry Laboratory Exercise. *J. Chem. Educ.* **2016**, 93, 2101–2105.

1983). Pure Appl. Chem. 1984, 56 (4), 461-466.

- (58) Aranzaes, J. R.; Daniel, M.-C.; Astruc, D. Metallocenes as References for the Determination of Redox Potentials by Cyclic Voltammetry Permethylated Iron and Cobalt Sandwich Complexes, Inhibition by Polyamine Dendrimers, and the Role of Hydroxy-Containing Ferrocenes. *Can. J. Chem.* **2006**, 84 (2), 288–299.
- (59) Sullivan, B. P.; Conrad, D.; Meyer, T. J. Chemistry of Highly Reduced Polypyridyl-Metal Complexes. Anion Substitution Induced by Ligand-Based Reduction. *Inorg. Chem.* 1985, 24 (22), 3640–3645.
- (60) Costentin, C.; Robert, M.; Savéant, J.-M. Concerted Proton-Electron Transfers: Electrochemical and Related Approaches. *Acc. Chem. Res.* **2010**, *43* (7), 1019–1029.
- (61) Liu, F.; Concepcion, J. J.; Jurss, J. W.; Cardolaccia, T.; Templeton, J. L.; Meyer, T. J. Mechanisms of Water Oxidation from the Blue Dimer to Photosystem II. *Inorg. Chem.* **2008**, *47* (6), 1727–1752
- (62) Cruz, A. J.; Kirgan, R.; Siam, K.; Heiland, P.; Rillema, D. P. Photochemical and Photophysical Properties of Ruthenium(II) Bis-Bipyridine Bis-Nitrile Complexes: Photolability. *Inorg. Chim. Acta* **2010**, 363 (11), 2496–2505.
- (63) Juris, A.; Balzani, V.; Barigelletti, F.; Campagna, S.; Belser, P.; von Zelewsky, A. Ru(II) Polypyridine Complexes: Photophysics, Photochemistry, Eletrochemistry, and Chemiluminescence. *Coord. Chem. Rev.* **1988**, *84*, 85–277.
- (64) Ngo, K. T.; Lee, N. A.; Pinnace, S. D.; Szalda, D. J.; Weber, R. T.; Rochford, J. Probing the Noninnocent π -Bonding Influence of N-Carboxyamidoquinolate Ligands on the Light Harvesting and Redox Properties of Ruthenium Polypyridyl Complexes. *Inorg. Chem.* **2016**, 55 (5), 2460–2472.
- (65) Cuéllar, E.; Méndez, A.; Pastor, L.; García-Herbosa, G.; Martín-Alvarez, J. M.; Miguel, D.; Villafañe, F. (1,2-azole) and/or (1,2-azolate) cis-bis(bipyridyl)ruthenium(II) Complexes. Manuscript in preparation.
- (66) Hameed, Y.; Gabidullin, B.; Richeson, D. Photocatalytic CO_2 Reduction with Manganese Complexes Bearing a K_2 -PN Ligand: Breaking the α -Diimine Hold on Group 7 Catalysts and Switching Selectivity. *Inorg. Chem.* **2018**, 57 (21), 13092–13096.
- (67) Valeur, B. Molecular Fluorescence. In *Digital Encyclopedia of Applied Physics*; Wiley-VCH Verlag GmbH & Co. KGaA: Weinheim, Germany, 2009; pp 477–531.

- (68) Baba, H.; Goodman, L.; Valenti, P. C. Solvent Effects on the Fluorescence Spectra of Diazines. Dipole Moments in the (n,π^*) Excited States 1. *J. Am. Chem. Soc.* **1966**, 88 (23), 5410–5415.
- (69) Cheung, P. L.; Machan, C. W.; Malkhasian, A. Y. S.; Agarwal, J.; Kubiak, C. P. Photocatalytic Reduction of Carbon Dioxide to CO and HCO₂H Using fac-Mn(CN)(bpy)(CO)₃. *Inorg. Chem.* **2016**, *55* (6), 3192–3198.
- (70) Rodrigues, R. R.; Boudreaux, C. M.; Papish, E. T.; Delcamp, J. H. Photocatalytic Reduction of CO_2 to CO and Formate: Do Reaction Conditions or Ruthenium Catalysts Control Product Selectivity? ACS Appl. Energy Mater. **2019**, 2 (1), 37–46.
- (71) Fujita, E.; Creutz, C.; Sutin, N.; Szalda, D. J. Carbon Dioxide Activation by Cobalt(I) Macrocycles: Factors Affecting CO₂ and CO Binding. *J. Am. Chem. Soc.* **1991**, *113* (1), 343–353.
- (72) Gennaro, A.; Isse, A. A.; Vianello, E. Solubility and Electrochemical Determination of CO₂ in Some Dipolar Aprotic Solvents. *J. Electroanal. Chem. Interfacial Electrochem.* **1990**, 289 (1–2), 203–215.
- (73) Dolomanov, O. V.; Bourhis, L. J.; Gildea, R. J.; Howard, J. A. K.; Puschmann, H. *OLEX2*: A Complete Structure Solution, Refinement and Analysis Program. *J. Appl. Crystallogr.* **2009**, *42*, 339–341.
- (74) Sheldrick, G. M. Crystal Structure Refinement with SHELXL. Acta Crystallogr., Sect. C: Struct. Chem. 2015, 71 (Md), 3–8.
- (75) Sheldrick, G. M. A Short History of SHELX. Acta Crystallogr., Sect. A: Found. Crystallogr. 2008, 64 (1), 112–122.
- (76) Nardelli, M. Parst: A System of Fortran Routines for Calculating Molecular Structure Parameters from Results of Crystal Structure Analyses. *Comput. Chem.* **1983**, *7*, 95–98.
- (77) Nardelli, M. PARST 95 an Update to PARST: A System of Fortran Routines for Calculating Molecular Structure Parameters from the Results of Crystal Structure Analyses. *J. Appl. Crystallogr.* **1995**, 28 (5), 659–659.
- (78) Jeffrey, G. A.; Lewis, L. Cooperative Aspects of Hydrogen Bonding in Carbohydrates. *Carbohydr. Res.* **1978**, *60* (1), 179–182.
- (79) Taylor, R.; Kennard, O. Comparison of X-ray and Neutron Diffraction Results for the N-H ···O = C Hydrogen Bond. *Acta Crystallogr., Sect. B: Struct. Sci.* 1983, 39 (1), 133–138.